Compressed Jahn-Teller Octahedra and Spin Quintet-Triplet Switching in Coordinatively Elastic Manganese(III) Complexes

SUNDARESAN, Sriram, KÜHNE, Irina A, EVESSON, Colin, HARRIS, Michelle M, FITZPATRICK, Anthony, AHMED, Ahmed, MÜLLER-BUNZ, Helge and MORGAN, Grace G

Polyhedron 208 (2021) 115386

Contents lists available at ScienceDirect

Polyhedron

journal homepage: www.elsevier.com/locate/poly

Compressed Jahn-Teller octahedra and spin quintet-triplet switching in coordinatively elastic manganese(III) complexes☆

Sriram Sundaresan [a,2], Irina A. Kühne [a,b,2], Colin Evesson [a], Michelle M. Harris [a], Anthony J. Fitzpatrick [a,1], Ahmed Ahmed [a], Helge Müller-Bunz [a], Grace G. Morgan [a,*]

[a] School of Chemistry, University College Dublin (UCD), Belfield, Dublin 4, Ireland
[b] FZU-Institute of Physics-Czech Academy of Sciences, Na Slovance 1999/2, 182 21 Prague 8, Czech Republic

ARTICLE INFO

Keywords:
Manganese
Schiff base
Spin crossover
Spin quintet
Spin triplet
Ligand rearrangement
Ring closure
Dimer

ABSTRACT

Complex assembly preferences and resultant spin state choice and Jahn-Teller distortion mode in twelve Mn(III) complexes of varying nuclearity with Schiff base chelate ligands of different sizes are compared. Mononuclear complexes Mn(5-F-Sal$_2$323)]OTf (**1**), [Mn(5-F-Sal$_2$323)]ClO$_4$ (**2**) and [Mn(5-F-Sal$_2$323)]NO$_3$, (**3**) with the 8-carbon R-Sal$_2$323 chelate type show rare axial compression at room temperature and complexes (**2**) and (**3**) also show reversible thermal spin state switching from spin quintet to triplet states on cooling. The prevalence of atypical axial compression is further probed by single crystal diffraction studies on high spin mononuclear complexes (**4**)-(**7**) with the longer 9-carbon R-Sal$_2$333 chelate series using [Mn(3-OEt-Sal$_2$333)]BF$_4$, (**4**) [Mn(3,5-diOMe-Sal$_2$333)]BF$_4$·0.5PrOH, (**5**), [Mn(5-F-Sal$_2$333)]BPh$_4$, (**6**) and Mn(5-NO$_2$-Sal$_2$333)]BPh$_4$, (**7**) as examples. Ring closure of both the 8-carbon R-Sal$_2$323 and longer 9-carbon R-Sal$_2$333 ligands was also observed yielding a ligand with a 6-membered ring in the mononuclear complex [Mn(3-OMe,5-NO$_2$-Sal$_2$333^{6R})]·0.07MeOH·0.93MeCN (**8**) in contrast to a protonated 5-membered ring in the dimeric complex [Mn$_2$(5-Cl-Sal$_2$323^{H5R})$_2$](ClO$_4$)$_2$·1.85EtOH·0.33MeCN, (**9**) with the R-Sal$_2$323 chelate type. Finally comparison of the assembly modes of Mn(III) complexes of the 8-carbon R-Sal$_2$323 and 9-carbon R-Sal$_2$333 series with those of the shorter 7-carbon R-Sal$_2$322 ligand series reveal that the mononuclear assembly mode is not favoured with the smaller chelate. Instead three dimeric or cluster complexes with rearranged ligands were recovered in low yield. The structures of these complexes [Mn$_2$(5-NO$_2$-Sal$_2$322^{5R})$_2$]·2BuOH, (**10**), [Mn$_2$(3,5-diBr-Sal$_2$322^{5R})(3,5-diBr-Sal)$_3$]·0.7EtOH·2.61MeCN, (**11**) and [Mn$_2$Na(3-NO$_2$,5-OMe-Sal$_2$322^{5R})]ClO$_4$·0.5MeCN (**12**) are reported and compared with examples with the longer chain R-Sal$_2$323 and R-Sal$_2$333 chelate ligands.

1. Introduction

The rich and facile redox chemistry of manganese in soft matter where it can span oxidation states from + 1 to + 7 mean it is ubiquitous in nature [1–7] and highly valued in catalysis [8–10]. Of equal importance is its role in the solid state where it is synonymous with single molecule magnetism [11,12] and highly valued in other applications including solar thermochemical energy conversion [13–15], colossal magnetoresistance [16–18] and ferroelectricity [19,20]. In many of these latter roles the Jahn-Teller distortion of trivalent manganese assumes a critical role in the function of the material, and the distortion is typically observed as an axial elongation due to population of the d_{z^2} orbital in the e_g* set. Indeed the success of manganese in underpinning the efficacy of many single molecule magnets is dependent on this feature of strong axial anisotropy [21–23]. Axial compression in spin quintet Mn(III) is more rare and the electronic structure of the few reported examples [24–39] has been the subject of sustained study in exemplary works by Tregenna-Piggot [24,25], Krzystek and Telser [26,36–38] and Duboc and Neese [27,28,34,35], who have built on the early work of Gregson [33] in establishing the sign and magnitude of the zero field splitting parameters. More rare again than axial compression of spin quintet Mn(III) is the spin triplet form of the ion, with only

☆ Part of the special issue dedicated to the element manganese, entitled Manganese: A Tribute to Chemical Diversity.

* Corresponding author.
E-mail address: grace.morgan@ucd.ie (G.G. Morgan).

[1] Current Address: Department of Biosciences and Chemistry, Sheffield Hallam University, Sheffield S1 1WB, UK.

[2] These authors contributed equally.

https://doi.org/10.1016/j.poly.2021.115386
Received 27 May 2021; Accepted 20 July 2021
Available online 29 July 2021

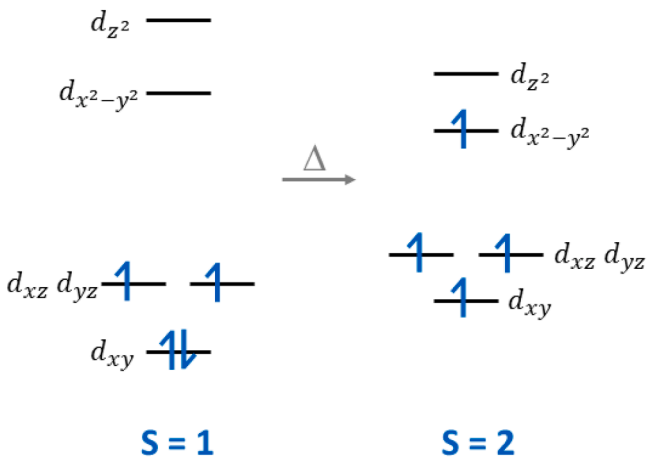

Fig. 1. Electronic splitting of octahedrally coordinated d^4 metal ions in the spin triplet form (left) and axially compressed spin quintet form (right).

around twenty known examples at room temperature. The S = 1 complexes are mostly $[Mn(CN)_6]^{3-}$ complexes with different counter cations [40–44], porphyrin [45–48] or cyclam [49] type ligands with axially coordinated ligands such as cyanide, poly(pyrazolyl)borate complexes [50–53] or a few with tris(quinone) oximate ligands [54], carboxylate donors [55], or hexadentate Schiff base ligands of the type discussed here [56]. Thermal switching between spin quintet and triplet forms of Mn(III) is also possible and has been reported with a small number of ligand types. Although the first example with tren pyrrole had an N_6 donor set [57], subsequent examples all showed an N_4O_2 donor set in a variety of skeletal frameworks [58–75], and all were recently reviewed by Olguin [76]. Chief among the N_4O_2 complexes are those with the hexadentate Schiff base ligand series resulting from condensation of 1,2-bis(3-aminopropylamino)ethane with a substituted 2-hydroxybenzaldehyde, often abbreviated as R-Sal$_2$323 to indicate the 323 8-carbon alkyl connectivity in the starting tetraamine and the substitution (R) on the phenolate ring. Such ligands are reported to stabilize an axially compressed environment in mononuclear manganese(III) examples when the ion is high spin, and we have suggested that the axial compression may assist the spin transition as the energetic order of orbitals matches that expected for the spin triplet form of the ion, Fig. 1 [59].

Here we investigate the co-existence of axial compression and spin triplet-quintet switching in three new examples of Mn(III) R-Sal$_2$323 complexes, [Mn(5-F-Sal$_2$323)]OTf (**1**), [Mn(5-F-Sal$_2$323)]ClO_4 (**2**) and [Mn(5-F-Sal$_2$323)]NO_3, (**3**) with the 8-carbon chelate type, see Scheme 1. These are compared with the assembly mode, local geometry and, where possible, the magnetic properties of complexes with the longer 9-carbon R-Sal$_2$333 and shorter 7-carbon R-Sal$_2$322 Schiff base analogues. Structural analysis suggests that the four complexes with the 9-carbon ligands [Mn(3-OEt-Sal$_2$333)]BF_4, (**4**) [Mn(3,5-diOMe-Sal$_2$333)]BF_4·0.5PrOH, (**5**), [Mn(5-F-Sal$_2$333)]BPh_4, (**6**) and Mn(5-NO_2-Sal$_2$333)]BPh_4, (**7**) are axially compressed like the R-Sal$_2$323 examples, but in contrast to the tighter 8-carbon chelate complexes, the 9-carbon complexes do not show thermal spin state switching. In complexation reactions with both the 8-carbon and 9-carbon ligands, Mn(III) complexes with rearranged ligands where the central alkylene spacer undergoes ring closure were also recovered, Scheme 1. With the R-Sal$_2$333 ligand type this yielded the mononuclear complex [Mn(3-OMe,5-NO_2-Sal$_2$333^{6R})·0.07MeOH·0.93MeCN (**8**), with the 6-membered ring closure indicated as "6R" in the formula, and with the R-Sal$_2$323 chelate type a dimeric complex [Mn_2(5-Cl-Sal$_2$323^{H5R})$_2$]$(ClO_4)_2$·1.85EtOH·0.33MeCN, (**9**) with a protonated 5-membered ring ("H5R")

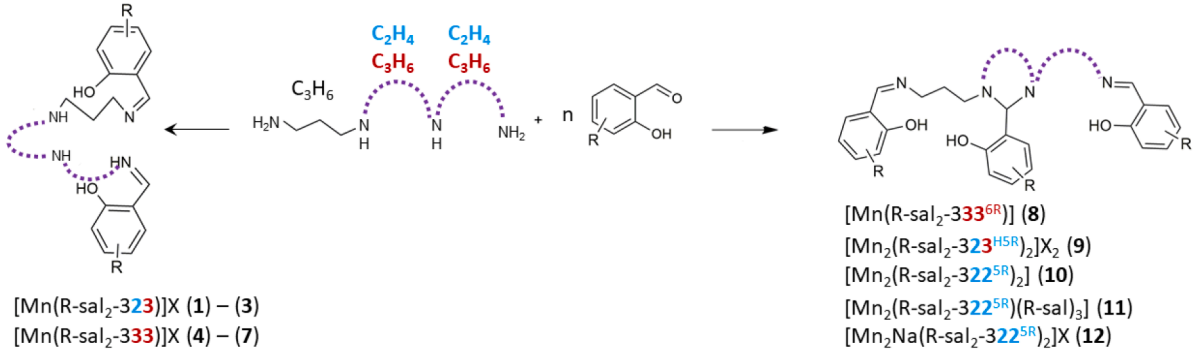

Scheme 1. General synthesis of the Schiff base ligands in compounds (**1**) - (**12**) with various lengths and combinations of the tetramine backbone and associated rearrangements.

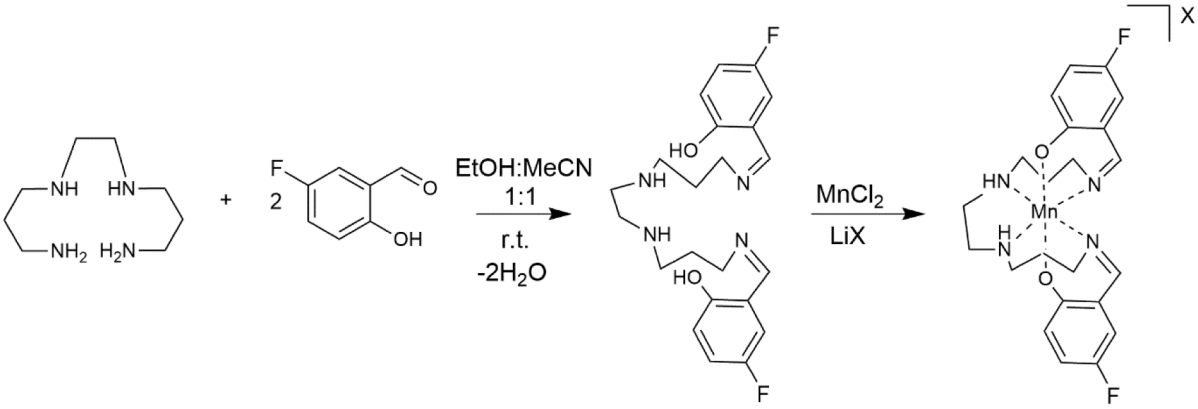

Scheme 2. Synthetic route for the preparation of complexes (**1**) - (**3**).

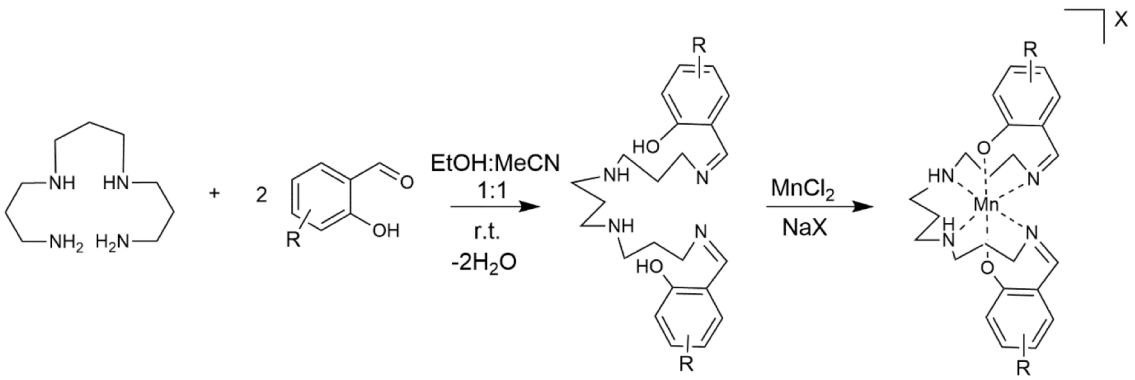

Scheme 3. Synthetic route for the preparation of complexes (**4**) - (**7**).

Table 1
Mn(III) complexes with R-Sal$_2$323, R-Sal$_2$333 and R-Sal$_2$322 Ligand Series.

323 Monomers	[Mn(5-F-Sal$_2$323)]CF_3SO_3	(**1**)
	[Mn(5-F-Sal$_2$323)]ClO_4	(**2**)
	[Mn(5-F-Sal$_2$323)]NO_3	(**3**)
333 Monomers	[Mn(3-OEt-Sal$_2$333)]BF_4	(**4**)
	[Mn(3,5-diOMe-Sal$_2$333)]BF_4·0.5PrOH	(**5**)
	[Mn(5-F-Sal$_2$333)]BPh_4	(**6**)
	[Mn(5-NO_2-Sal$_2$333)]BPh_4	(**7**)
333^{6R} Monomer	[Mn(3-OMe,5-NO_2-Sal$_2$333^{6R})]·0.07MeOH·0.93MeCN	(**8**)
323^{H5R} Dimer	[Mn_2(5-Cl-Sal$_2$323^{H5R})$_2$]$(ClO_4)_2$·1.85EtOH·0.33MeCN	(**9**)
322^{5R} Dimer	[Mn_2(5-NO_2-Sal$_2$322^{5R})$_2$]·2BuOH	(**10**)
322^{5R} Dimer	[Mn_2(3,5-diBr-Sal$_2$322^{5R})(3,5-diBr-Sal)$_3$]·0.7EtOH·2.61MeCN	(**11**)
322^{5R} Na@Dimer	[Mn_2Na(3-NO_2,5-OMe-Sal$_2$322^{5R})$_2$]ClO_4·0.5MeCN	(**12**)

was recovered, Scheme 1. Finally, we also examined the effect of shortening the skeletal framework supporting the N_4O_2 donor set by preparing ligands with the 7-carbon R-Sal$_2$322 ligand type. This new ligand series was also of interest as it is asymmetric in contrast to the 8-carbon R-Sal$_2$323 and 9-carbon R-Sal$_2$333 Schiff bases. Introduction of an asymmetric framework could be useful in discerning if the distortion observed in the Mn(III) complexes with the symmetric 8-carbon R-Sal$_2$323 and 9-carbon R-Sal$_2$333 is a genuine compression or an accident of the residual symmetry of the coordination sphere in the complexes with the symmetric ligands where there are only two unique axes: 1xO-Mn-O and 2xN_{amine}-Mn-N_{imine} [59]. However the study revealed that mononuclear Mn(III) chelate formation is disfavoured with the 7-carbon R-Sal$_2$322 ligand type and three dimeric or cluster complexes with rearranged ligands were recovered instead, see Scheme 1. Although yields were too low to enable magnetic investigation, the structures of all three [Mn_2(5-NO_2-Sal$_2$322^{5R})$_2$]·2BuOH, (**10**), [Mn_2(3,5-diBr-Sal$_2$322^{5R})(3,5-diBr-Sal)$_3$]·0.7EtOH·2.61MeCN, (**11**) and [Mn_2Na(3-NO_2,5-OMe-Sal$_2$322^{5R})]ClO_4 ·0.5MeCN (**12**) could be determined and are reported here.

2. Results and discussion

The synthesis of Mn(III) complexes with members of each of the three ligand types R-Sal$_2$323, (Scheme 2) R-Sal$_2$333 (Scheme 3) and R-Sal$_2$322 (Scheme 6) was investigated using a Mn(II) salt followed by air oxidation. This yielded mononuclear complexes (**1**)-(**3**) and (**4**)-(**7**) with R-Sal$_2$323 and R-Sal$_2$333 respectively. In addition, products (**8**) and (**9**) with ligand rearrangements of the 8-carbon and 9-carbon ligand types were also obtained. Attempted complexations with the 7-carbon R-Sal$_2$322 ligand family only yielded crystalline products (**10**)-(**12**) with the ring closed rearranged ligand R-Sal$_2$322^{5R}. The formulae of all products (**1**)-(**12**) are listed in Table 1 in the order in which they are reported, and each family is discussed in turn below.

2.1. 323 Monomers complexes (1)-(3) – Synthesis, magnetism and structural analysis

The reaction of 5-fluorosalicylaldehyde with 1,2-bis(3-aminopropylamino)ethane (3 2 3) in a 2:1 ratio led to the formation of a hexadentate Schiff base ligand of suitable geometry to chelate a Mn(III) centre. This resulted in the formation of dark red/black crystals of complexes (**1**) - (**3**) which were prepared in a one-pot synthesis, Scheme 2. The structures of these three compounds were established by single crystal X-ray diffraction

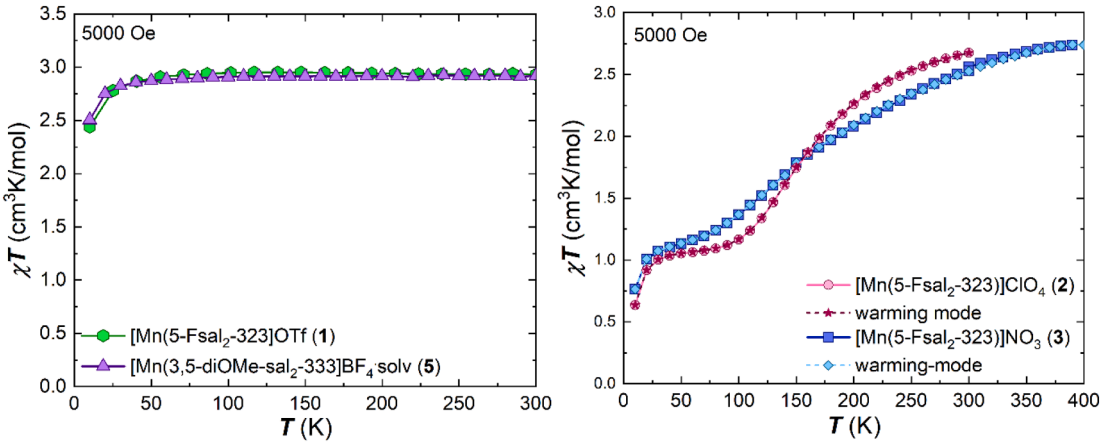

Fig. 2. Plots of χ_MT versus T for the two high-spin complexes (**1**) (green) and (5) (purple) (left) in cooling mode, and the two SCO complexes (**2**) (pink) and (**3**) (blue) in the temperature range 5–300 K in cooling and warming mode. ((Colour online.))

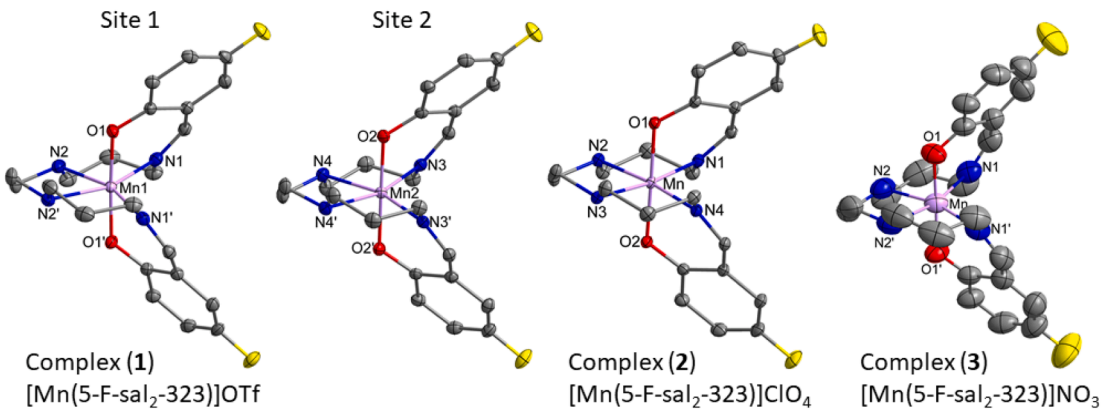

Fig. 3. Molecular structures of complexes (**1**) - (**3**); measured at 100 K for (**1**) and (**2**), and at 293 K for (**3**), respectively. (Hydrogen atoms and solvent molecules omitted for clarity).

Table 2
Mn-donor bond lengths in complexes (**1**) - (**3**).

Mn-X	Complex (**1**)		Complex (**2**)	Complex (**2**)	Complex (**3**)
Temperature	100 K		100 K	293 K	293 K
	Mn1	Mn2			
Mn-O_{phen}	1.8690(10)	1.8674(9)	1.8865(7)	1.8817(11)	1.8699(14)
			1.8876(8)	1.8833(11)	
Mn-N_{imine}	2.1035(12)	2.1093(11)	1.9976(9)	2.0936(14)	2.0723(19)
			1.9905(9)	2.0644(14)	
Mn-N_{amine}	2.2461(12)	2.2231(12)	2.0669(9)	2.1617(15)	2.172(2)
			2.0650(9)	2.1876(15)	
spin state	S = 2	S = 2	S = 1	S = 2	S = 2

and the bulk samples were then fully characterized using elemental analysis, IR spectroscopy and magnetic measurements. Complexes (**1**) - (**3**) all crystallize as mononuclear Mn(III) species with an octahedral ligand environment. Complex (**1**) was formed by a salt metathesis procedure using lithium triflate, while compounds (**2**) and (**3**) were prepared using the respective Mn(II) salt. This method led to the successful crystallization of the desired cationic Mn(III) species: [Mn(5-F-$Sal_2$323)]OTf (**1**), [Mn(5-F-$Sal_2$323)]ClO_4 (**2**) and [Mn(5-F-$Sal_2$323)]NO_3, (**3**).

The magnetic properties of the dried complexes (**1**) – (**3**) and (**5**) (for synthesis and structure of (**5**) see Section 2) were determined using SQUID magnetometry and the data were collected from 300.0 K down to 5.0 K under an applied dc field of 5000 Oe, Fig. 2. The data for complex (**5**) are included here as it was the only member of the R-$Sal_2$333 series for which magnetic properties were investigated. Only in the case of complex (**3**) were the susceptibility data collected up to 400 K. No thermal hysteresis was detected on warming back to room temperature in the cases of compounds (**2**) and (**3**), and plots of $\chi_M T$ versus T are shown in Fig. 2.

Complexes (**1**) and (**5**) are in the spin quintet form over the whole measured temperature range with $\chi_M T$ values close to the expected spin only value of 3.0 cm^3K/mol for a monomeric Mn(III) complex with S = 2 and g = 2. On the other hand, both complexes (**2**) and (**3**) exhibit an incomplete thermal spin transition. Below 100 K both exist in the spin triplet form with $\chi_M T$ values close to the expected spin-only value of 1.0 cm^3K/mol for S = 1, assuming g = 2. Above 100 K both show SCO upon warming, with a gentle sigmoidal pathway, although neither reaches the pure high-spin state by 300 K (expected spin-only value of 3.0 cm^3K/mol for S = 2). $T_{1/2}$ values were determined to be 172 K for (**2**) and 190 K for (**3**).

The crystal structure of complex (**1**) was analysed at 100 K and was solved in the monoclinic space group $P2/c$ with Z = 4. The structure of complex (**2**) was determined at 100 K and at room temperature (293 K) and was solved in both cases in the triclinic space group $P\bar{1}$ with Z = 2. Therefore, no phase transition, which can often be observed upon spin transition [66], is detectable. This is in contrast to the [Mn(5-F-$Sal_2$323)]ClO_4 mononuclear complex from Wang et al. [75] who have recently reported a polymorph of the same complex with the same structural formula but which crystallizes in the monoclinic space group $P2_1/c$. The magnetic profiles of the two polymorphs are distinctly different with $T_{1/2}$ values shifted from 100 K in [75] to 172 K for complex (**2**). The structure of complex (**3**) was determined at 293 K and the crystals were found to be in the orthorhombic space group *Pccn* with Z = 4, while a 100 K structure could not be collected due to constant breaking of the crystals, which is possibly caused by a structural phase transition. The complete crystallographic details for compounds (**1**) - (**3**) can be found in Tables A1-A2 in the Appendix. The structures of the complex cations in each of (**1**) - (**3**) are shown in Fig. 3 and the asymmetric unit varies for each. The asymmetric unit of compound (**1**) contains half of each of two Mn(III) complex cations each with an internal C_2 axis and one full triflate anion. The asymmetric unit of complex (**2**) comprises one full Mn(III) complex cation and one full perchlorate anion at both measured temperatures, while that for complex (**3**) has half of one [Mn(5-F-$Sal_2$323)]$^+$ cation and half of a nitrate anion, both with C_2 axis.

The hexadentate Schiff base ligand chelates the Mn(III) centre in *pseudo* octahedral geometry with two *trans*-phenolate donors, two *cis*-amine and two *cis*-imine donor atoms, which is similar to other Mn(III) compounds using related hexadentate ligands that can undergo spin transition [58–67,76]. Within such Mn(III) SCO compounds, the bond length changes which accompany the spin transition, are only significant for the amine and imine bond lengths in the equatorial positions, while the Mn-O distance stays constant. The usually observed Mn-N bond lengths are given below:[58,61]

	S = 1	S = 2
Mn-N_{amine}	2.00–2.10 Å	2.20–2.30 Å
Mn-N_{imine}	1.95–2.00 Å	2.10–2.15 Å

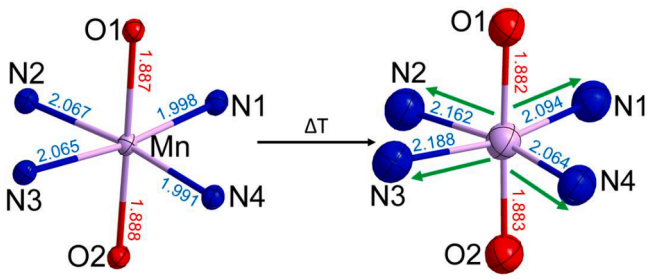

Fig. 4. Bond length changes within complex (**2**) from 100 K (left) to room temperature, 293 K (right).

The bond lengths of compounds (**1**) - (**3**) are summarized in Table 2. The long Mn-N_{imine} and Mn-N_{amine} bond lengths found within complex (**1**) and the room temperature structures of (**2**) and (**3**) clearly indicate the spin-quintet state which is consistent with the observed magnetic properties. Only the 100 K structure of (**2**) exhibits bond lengths that are indicative of a spin-triplet state and these change upon temperature increase for both sets of Mn-N bonds, see Fig. 4, highlighting the axial compression in the spin quintet form.

2.2. 333 Monomers complexes (4) - (7) – Synthesis and structural analysis

The reaction of substituted salicylaldehydes in a 2:1 ratio with the longer tetraamine, 1,3-bis(3-aminopropylamino)-propane (333), led to the formation of a variety of Schiff base ligands, which are also suitable hexadentate ligands to chelate a Mn(III) centre in mononuclear mode. This resulted in the formation of dark red/black crystals of complexes (**4**) - (**7**) which were also prepared in a one-pot synthesis, Scheme 3. In a similar way as for the first three complexes, (**4**) – (**7**) all crystallize as mononuclear Mn(III) species with an octahedral ligand environment. Complexes (**4**) – (**7**) were formed by a salt metathesis procedure with the target counterions introduced as their group 1 salts, for example sodium as indicated in Scheme 3.

This method led to the successful crystallization of the desired cationic Mn(III) species with tetraphenylborate, BPh_4^-, and tetrafluoroborate, BF_4^-, respectively, with the following formulae: [Mn(3-OEt-$Sal_2$333)]BF_4 (**4**), [Mn(3,5-diOMe-$Sal_2$333)]BF_4•0.5C_3H_8O (**5**), [Mn(5-F-$Sal_2$333)]BPh_4 (**6**) and [Mn(5-NO_2-$Sal_2$333)]BPh_4 (**7**). Compounds (**4**), (**6**) and (**7**) crystallize without any solvent molecules in the crystal lattice. The complete crystallographic details for compounds (**4**) – (**7**) can be found in Tables A2 and A3 in the Appendix. Only complex (**5**) was modelled with solvent, in this case half a molecule of propanol in the crystal lattice. The solvent molecule itself could not be determined crystallographically in the diffraction experiments in terms of atomic sites, therefore Platon SQUEEZE [77] was used to compensate for the spread electron density. The structures of the cation–anion combinations for compounds (**4**) – (**7**) are shown in Fig. 5.

The structure of complex (**4**) was determined in the triclinic space group $P\bar{1}$ with Z = 2, while the structures of both complexes (**5**) and (**6**) were solved in the monoclinic space group $P2_1/c$ with Z = 2 (for (**5**)) and Z = 4 (for (**6**)). Complex (**7**) was found to crystallize in the orthorhombic space group $Pna2_1$ with Z = 4. The asymmetric unit contains, in all four cases, one full [MnR-$Sal_2$333]$^+$ cation and one full anion, respectively, Fig. 5. The arrangement of donor atoms in the R-$Sal_2$333 complexes follows the pattern observed in the R-$Sal_2$323 block, *i.e.* two *trans*-phenolate donors, two *cis*-amine and two *cis*-imine donor atoms. We have recently shown that the binding amine nitrogen atoms can have their hydrogen atoms either both pointing in the same direction leading to the *meso* form, or in opposite directions, leading to the non-*meso* form, in Fe(III) complexes with R-$Sal_2$333 ligands [78]. In the Mn(III) complexes reported here with R-$Sal_2$333 Schiff base ligands, the non-*meso* form is favoured as seen in complexes (**4**) – (**6**), Fig. 5, and co-crystallization of the non-*meso* and *meso*-forms is only observed in the tetraphenylborate complex (**7**). Crystallographic analysis reveals that the non-*meso* nitrogen atom, N3A, is dominant, with a site occupation factor of 0.79, while the *meso* nitrogen atom, N3B, plays a minor role.

The bond lengths for complexes (**4**) – (**7**) are summarized in Table 3, and the long Mn-N donor lengths suggest a spin state assignment of S = 2 in all cases. All show short bond lengths to the phenol oxygen atoms in the range between 1.85 and 1.89 Å and this is the strongest indication of

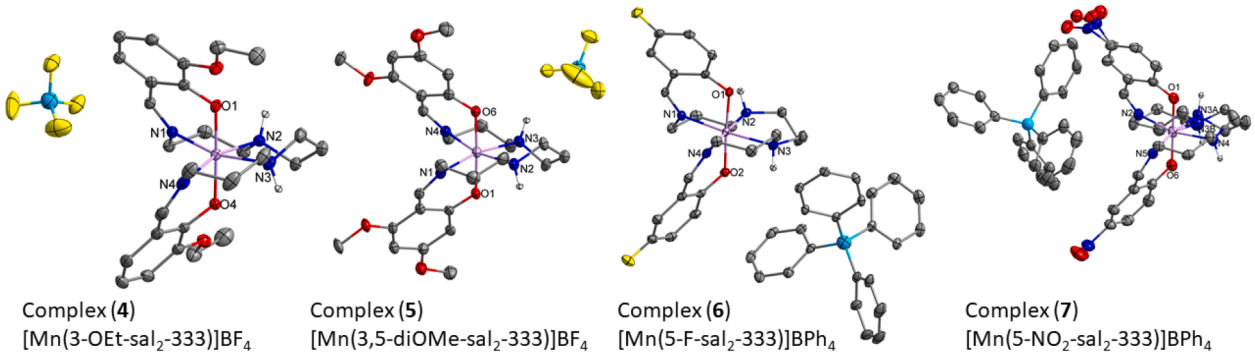

Fig. 5. Molecular structures of complexes (**4**) – (**7**). (Hydrogen atoms and solvent molecules omitted for clarity).

Table 3
Mn-donor bond lengths in complexes (**4**) – (**8**).

Mn-X	Complex (**4**)	Complex (**5**)	Complex (**6**)	Complex (**7**)	Complex (**8**)
Mn-O_{phen}	1.8719(10)	1.883(3)	1.8557(8)	1.881(2)	1.8739(8)
	1.8820(10)	1.894(3)	1.8650(8)	1.875(2)	1.8774(8)
					2.0966(9)
Mn-N_{imine}	2.0971(11)	2.073(4)	2.0894(10)	2.143(3)	2.1171(10)
	2.1711(12)	2.143(4)	2.1645(9)	2.109(3)	2.1779(10)
Mn-N_{amine}	2.2385(12)	2.198(4)	2.1931(10)	2.23(3)[a]; 2.234(5)[a]	2.2939(10)
	2.3273(12)	2.315(4)	2.2602(10)	2.292(3)	
spin state	S = 2	S = 2	S = 2	S = 2	S = 2

a) complex (**7**) exhibits a disorder around N3 with site occupation factors 0.78(N3A):0.21(N3B).

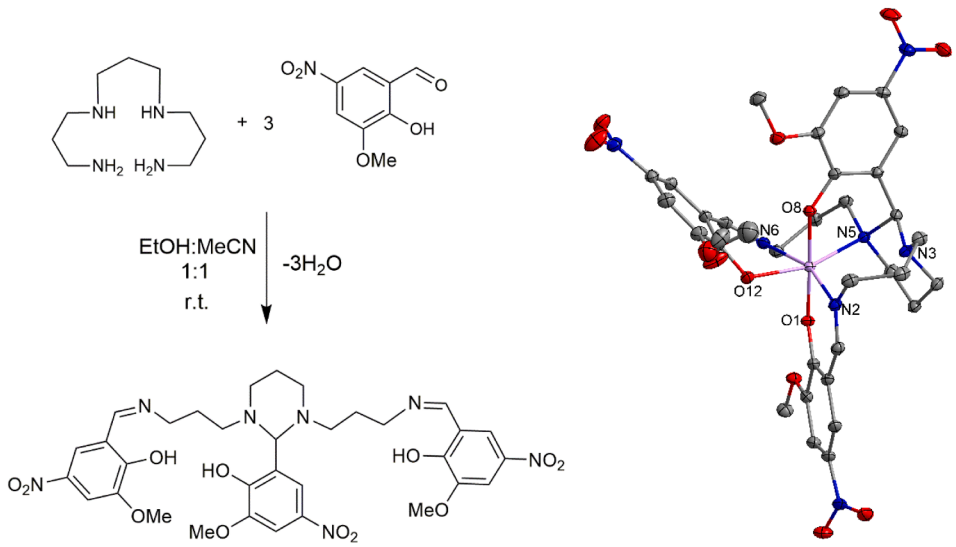

Fig. 6. Ligand rearrangement during the Schiff base reaction (left), and the molecular structure of [Mn(3-OMe,5-NO_2-Sal_2333^{6R})]·0.07MeOH·0.93MeCN (**8**), (right) (Hydrogen atoms and solvates omitted for clarity).

Table 4
Distortion angle parameters, Σ (angular deviation at the origin) and Θ (trigonal torsion angle) for all mononuclear Mn(III)complexes (**1**) – (**8**).

	(1) [Mn(5-F$Sal_2$323)]X		(2)	(2)	(3)	(4) [Mn(R-$Sal_2$333)]X	(5)	(6)	(7)	(8) [$Mn333^{6R}$]
T(K)	100		100	293	293	100	100	100	100	100
Σ	72.5°	63.8°	29.3°	48.9°	61.2°	72.2°	57.1°	46.4°	61.5°*	79.8°
Θ	258.6°	217.3°	91.8°	170.9°	189.8°	251.1°	196.9°	146.4°	203.5°*	282.1°
State	S = 2	S = 2	S = 1	S = 2	S = 2	S = 2	S = 2	S = 2	S = 2	S = 2

*The disorder of complex (**7**) around N3 (s.o.f.: 0.78(N3A):0.21(N3B)): distortion using N3B: Σ = 80.6° and Θ = 297.0°.

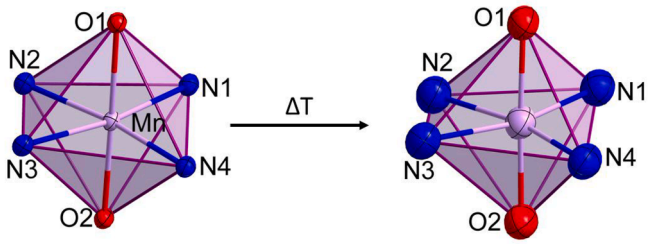

Fig. 7. Change of the octahedral environment within complex (**2**) from 100 K (left) to room temperature, 293 K (right).

an axial compression. The distortion is harder to define when considering only the pairs of Mn-N_{imine} and Mn-N_{amine} distances as there are significant differences between the imine-amine sets in non-*meso* complexes (**4**) – (**6**). All are, however, typical for high-spin Mn(III) complexes, where the average bond lengths from literature are given as Mn-N_{imine} 2.1–2.2 Å and Mn-N_{amine} 2.2–2.3 Å [58,61].

2.3. 333^{6R} Monomer complex (8) – Synthesis and structural analysis

We have also recovered a crystalline by-product, complex (**8**), with the 3-OMe,5-NO_2-$Sal_2$333 ligand where the ligand has undergone ring closure. In this case the two secondary amines of the tetraamine backbone undergo an additional condensation reaction with one salicylaldehyde, leading to a six-membered ring as depicted in Fig. 6, leading to the formation of the Schiff base ligand 3-OMe,5-NO_2-Sal_2333^{6R}. Complex (**8**), [Mn(3-OMe,5-NO_2-Sal_2333^{6R})]·0.07MeOH·0.93MeCN, is the only example of a 333-rearrangement we encountered using this type of reaction leading to a 6-membered ring closure, in contrast to the 5-membered rings obtained with rearrangements of R-$Sal_2$323 and R-$Sal_2$322 in some of the complexes described in the following sections. Complex (**8**) crystallizes as a mononuclear species with an octahedral environment provided by an N_3O_3 donor set, see Fig. 6.

In the literature, a similar formation of a hexahydropyrimidine ring, has been observed before when using the smaller *N,N'*-bis(2-aminoethyl)-1,3-propanediamine (2,3,2-tetramine) [79], whereas in our case, the central propyldiamine part is condensed with one aldehyde. Complex (**8**) crystallizes with one solvent molecule in the crystal lattice as a neutral mononuclear species with one fully deprotonated ligand, [MnL1]•0.93MeCN•0.07MeOH, in the triclinic space group $P\bar{1}$ with Z = 2 and the molecular structure is shown in Fig. 6. The complete crystallographic details for compound (**8**) can be found in Table A3 in the Appendix. The transformed Schiff base ligand chelates the Mn(III) centre in *pseudo* octahedral geometry. The coordination sphere around the Mn (III) consists of three phenol oxygen atoms (O1, O8 and O12), two imine nitrogen atoms (N2 and N6), and one amine nitrogen atom, N5, which is part of the hexahydropyrimidine ring, while the second nitrogen atom of the ring closure, is not coordinated. The three oxygen donors, as well as the three nitrogen donors are arranged in a *mer*-conformation. The bond lengths of (**8**) are summarized in Table 3, to highlight the similarity to compounds (**4**) – (**7**). The bond lengths of the axial phenol oxygen atoms, O1 and O8, are in a similar range as within compounds (**4**) - (**7**), while the one oxygen atom in the equatorial position, O12, is 0.2 Å longer. The Mn-N bond lengths to the imine and amine nitrogen donors are also similar to the ones observed in compounds (**4**) – (**7**). The distance between the central Mn(III) ion and the uncoordinated tertiary amine, N3, is 2.92 Å.

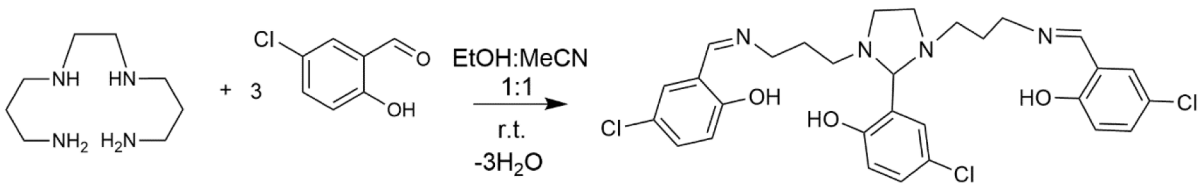

Scheme 4. Ligand rearrangement using 323-tetramine and 5-chlorosalicylaldehyde.

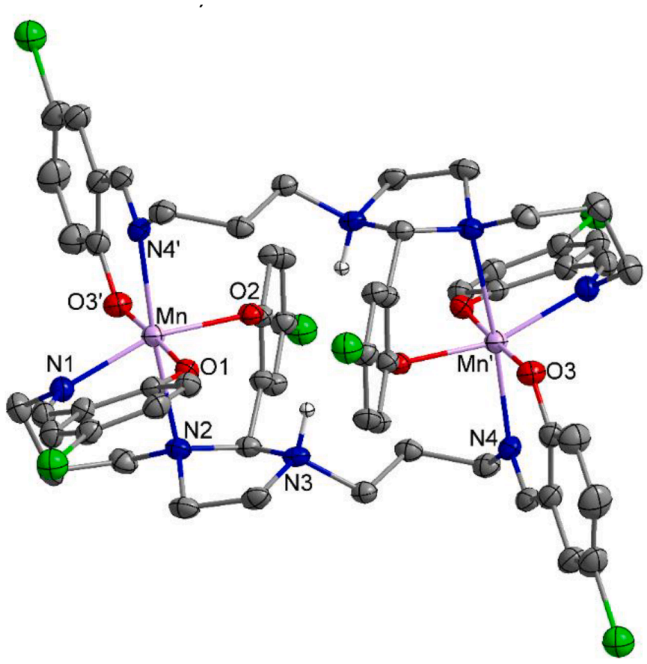

Fig. 8. Molecular structure of complex (**9**) (the majority of hydrogen atoms are omitted for clarity; the symmetry generated atoms are indicated by a dash; symmetry code: 1-x, 1-y, 1-z).

2.4. Distortion parameters in 323 Monomers (1)-(3) and 333/333^{R} Monomers (4)-(8)

Mn(III) complexes of the R-Sal$_2$323 type exhibit strong Jahn-Teller distortion of the octahedral environment in the spin quintet form while the spin triplet form is usually almost perfectly behaved. The degree of distortion can be analysed by the distortion parameters Θ and Σ as defined by McKee et al. [80] where Σ measures the angular deviation (from the *cis* octahedral angles of 90°), while Θ measures the trigonal torsion. Σ and Θ have been reported in the literature with values of Σ = 28° − 45° and Θ = 79° − 125° for Mn(III) compounds in the S = 1 spin state and Σ = 48° − 80° and Θ = 135° − 230° for the S = 2 form [61,63]. Here Σ and Θ have been calculated using OctaDist 2.6.1 [81], and the observed parameters are summarized in Table 4 and show the structural distortion due to the different spin states of the complexes. Only the 100 K structure of complex (**2**) exhibits Σ and Θ values in the range expected for spin triplet Mn(III), which is in good agreement with the magnetic properties, which change upon increase in temperature to values typical for spin quintet Mn(III), *i.e.* with greater distortion of the octahedral environment around the Mn(III) center (Fig. 7). All other monomeric Mn(III) complexes, including that with the rearranged 333^{6R} ligand show Σ and Θ values indicative of an S = 2 spin state. The distortion parameters, Σ and Θ, for the monomeric complex (**8**) with the rearranged Schiff base ligand were determined, Table 3, highlighting the distortion from the perfect octahedral environment, but they were observed to be in a similar range as those found in compounds (**4**) – (**7**).

Analysis of the Σ values of spin triplet and spin quintet forms of [Mn(R-Sal$_2$323)]$^+$ complexes has revealed that those with Σ values above 70° are often, but not always, locked in the high-spin state [76]. We have recently highlighted that comparison of the Θ values might be a better indicator to identify those examples for which spin transition will be blocked because the change in distortion between the two spin forms is too high [58,82]. Application of the same rationale to the [Mn(R-Sal$_2$333)]$^+$ complex cations would suggest that compound (**6**) might be capable of spin state switching even though the bond lengths at 100 K indicate that it is still in the quintet form. It is clear that several factors must come together to facilitate the large geometric changes associated with the spin state change and associated loss/gain in Jahn-Teller distortion in d^4. Axial compression of the spin quintet form may, however, be critical in facilitating the change.

2.5. 323^{5R} Dimer complex (9) – Synthesis and structural analysis

When using the R-Sal$_2$323 ligand, we observe in the majority of cases the formation of the expected mononuclear Mn(III) complex [58–67]. In one case, we have now found a similar ring closure when using the 323-tetramine, but instead of forming a hexadentate Schiff base ligand as seen within compounds (**1**) - (**3**), the central ethylenediamine unit can undergo a ring closure leading to a 5-membered ring, see Scheme 4. This type of 5-membered ring-formation has been observed when using various lengths of ethylenediamine [83–85], and is especially well-known for the symmetric triethylenetetramine with various substituted benzaldehydes [86–92]. It can also be observed when using longer multi-amine chains such as tetraethylenepentamine and pentaethylenehexamine [93–96].

Using 5-chlorosalicylaldehyde and the 323-tetramine as depicted in Scheme 4, we observed the rearranged Schiff base ligand, 5-Cl-Sal$_2$323^{5R}, and the crystallization of complex (**9**) in the trigonal space group P$\bar{3}$ with Z = 9 as a dimeric Mn(III) compound with two octahedrally coordinated Mn(III) ions each with an N_3O_3 donor set. The complete crystallographic details for compound (**9**) can be found in Table A4 in the Appendix.

Each of the two rearranged Schiff base ligands chelates the two Mn

Table 5
Comparison of the Mn-donor bond lengths within complexes (**9**) and (**10**) (in Å).

Complex (**9**)	Mn		Complex (**10**)	Mn1		Mn2	
L2 Mn-O_{phen}	Mn-O1	1.8719(13)	L3 Mn-O_{phen}	Mn1-O6	1.871(2)	Mn2-O9	1.899(3)
	Mn-O3′	1.8630(13)		Mn1-O18	1.885(2)	Mn2-O15	1.869(2)
	Mn-O2	1.9813(12)		Mn1-O1	2.092(2)	Mn2-O10	2.087(3)
L2 Mn-N_{imine}	Mn-N1	2.0562(15)	L3 Mn-N_{imine}	Mn1-N13	2.036(3)	Mn2-N6	2.039(3)
	Mn-N4′	2.2030(14)		Mn1-N2	2.070(3)	Mn2-N9	2.057(3)
L2 Mn-N_{amine}	Mn-N2	2.4938(14)	L3 Mn-N_{amine}	Mn1-N3	2.340(3)	Mn2-N10	2.349(3)

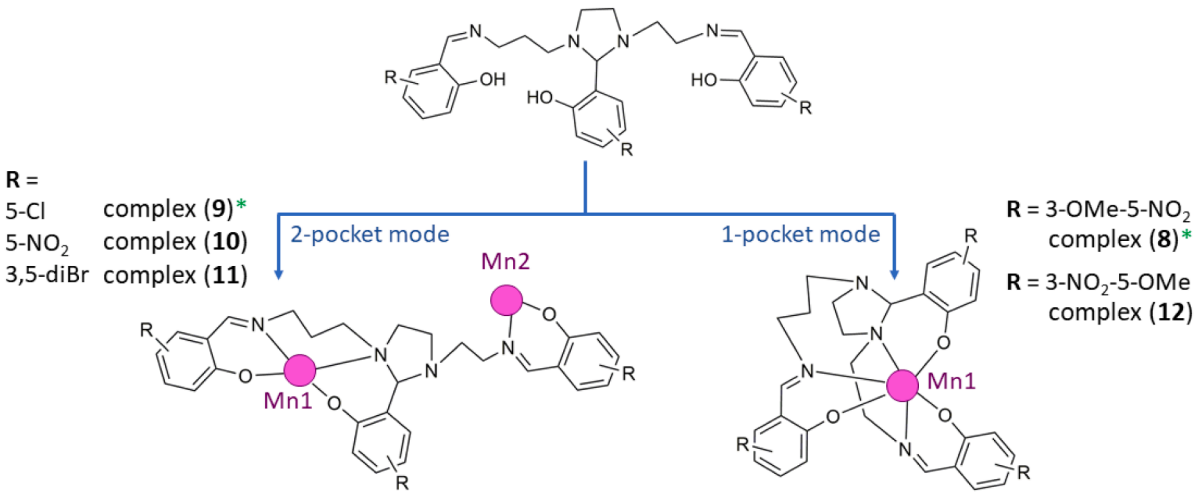

Scheme 5. Pocket formation of the rearranged Schiff base ligand based on the 322-tetramine, to incorporate either two Mn(III) metal centers (left) or only one (right).(NB: complex (**8**) and (**9**) are not based the 322-tetramine, but use the 333-tetramine (**8**) and 323-tetramine (**9**), respectively, marked with a green asterisk).

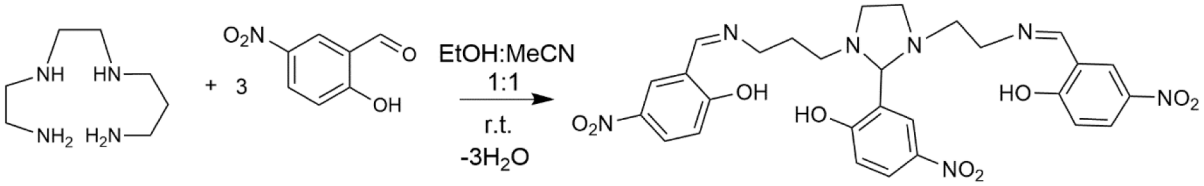

Scheme 6. Ligand rearrangement using the 322-tetramine together with 5-nitrosalicylaldehyde.

(III) centers, leading to a head-to-tail arrangement of the two ligands. The dimeric molecule crystallizes with 1.85 molecules of ethanol and 0.33 molecules of acetonitrile within the crystal lattice. While the phenolate oxygen atoms of 5-Cl-Sal$_2$323^{5R} are fully deprotonated, the ligand exhibits a protonation of the uncoordinated nitrogen atom of the 5-membered ring, N3, in protonated ligand 5-Cl-Sal$_2$323^{H5R} which therefore requires two perchlorate anions for charge balance in the crystal lattice, leading to a molecular formula of [Mn$_2$(5-Cl-Sal$_2$323^{H5R})$_2$](ClO$_4$)$_2$·1.85EtOH·0.33MeCN (**9**). The structure of (**9**) is shown in Fig. 8 and displays an inversion center in the middle of the molecule, leading to a distance between the two Mn(III) centers of 6.58 Å, see Table 5.

Both Mn(III) centers are octahedrally coordinated and exhibit an N_3O_3 donor set, which is provided by the two rearranged Schiff base ligands. The coordination sphere around the Mn(III) centers is built up by the three phenol oxygens O1, O2 and O3, the imine nitrogens N1 and N4, and amine nitrogen atom of the 5-membered ring, N2, and the corresponding bond lengths are summarized in Table 5. The three oxygen donors, as well as the three nitrogen donors are arranged in a *mer*-conformation, with two axially positioned Mn-O bonds, Mn-O1 and Mn-O3′, with lengths of 1.86–1.87 Å, which are shorter than the third bond to O2, which is about 0.11 Å longer.

The shorter axial Mn-O$_{phen}$ bond lengths resemble those observed within the SCO complexes (**1**) – (**3**), whereas the two Mn-N$_{imine}$ bond lengths show more similarity with the trend observed in (**4**) – (**7**), with one shorter Mn-N1 bond and one longer Mn-N4′, with a bond distance difference of about 0.15 Å. The bond length to the amine nitrogen atom of the 5-membered ring, N2, is at 2.49 Å rather long, and certainly longer than observed within any of the compounds described herein.

3. Observed rearrangements and pocket formation

The electron-withdrawing substituents on the salicylaldehyde, such as nitro or halide groups, seem to support the ligand rearrangements observed within complexes (**8**) and (**9**). These two compounds show the two different chelation modes of the rearranged Schiff base ligands highlighting the high degree of flexibility available to incorporate Mn (III) centers by forming various pockets, see Scheme 5.

As observed within the dimeric compound (**9**), the ligand can exhibit the two-pocket-mode, where the first pocket provides four donors to one Mn(III) center using two of the three salicylaldehyde moieties of the ligand. The second pocket is then formed by one salicylaldehyde which provides a phenolate oxygen and an imine nitrogen donor. Two ligands are then arranged in a head-to-tail fashion to provide the octahedral environment for the Mn(III) ions.

On the other hand, the rearranged Schiff base ligand can also wrap around one single Mn(III) center, 1-pocket mode in Scheme 5, as seen within the monomeric complex (**8**), using all three oxygen donors, both

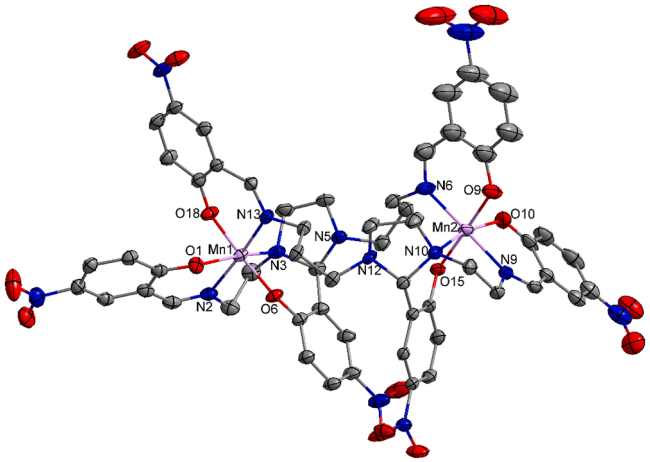

Fig. 9. Molecular structure of complex (**10**) (hydrogen atoms and solvates are omitted for clarity).

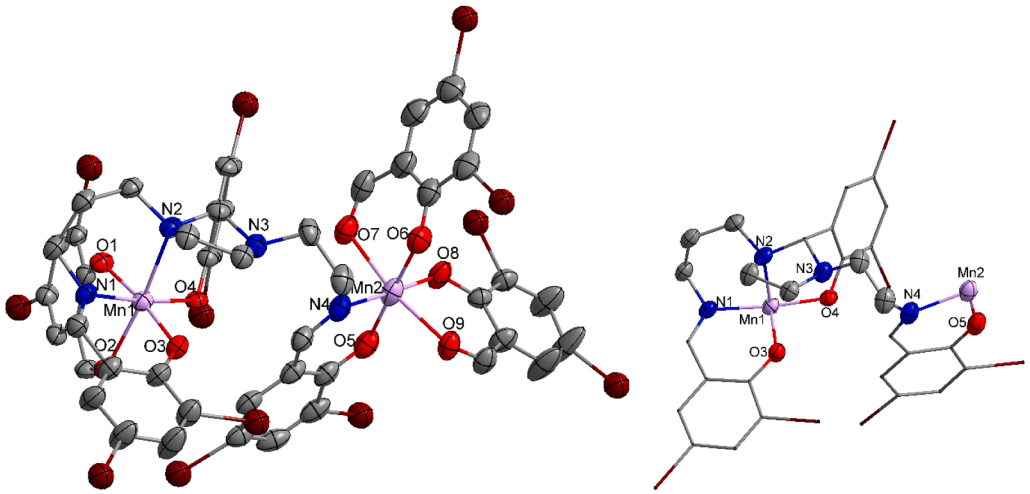

Fig. 10. Molecular structure of complex (**11**) (left) ligand coordination of the deprotonated rearranged Schiff base ligand, 3,5-diBr-Sal$_2$322^{5R} (right) (Hydrogen atoms omitted for clarity).

imine nitrogen donors as well as one of the tertiary amine nitrogen donors of the enclosed ring. Using the longer 333-tetramine backbone might be helpful to encapsulate one single Mn(III) center, but we will show within complex (**12**) that even the shorter 322-tetramine backbone can arrange this way, highlighting the great flexibility of this framework.

3.1. 322^{5R} dimeric complexes (10)-(12) – Synthesis and structural analysis

While we only observed one example with the rearranged 333-tetramine ligand, complex (**8**), and one with the 323-tetramine ligand, complex (**9**), such rearrangements seem to happen more frequently when using the asymmetric and shorter 322-tetramine. Similarly to the rearrangement observed within complex (**9**), the shorter 322-tetramine rearranges *via* the same 5-membered ring-closure on the central ethylenediamine unit, as depicted in Scheme 6. We were able to isolate three complexes (**10**) - (**12**) in small quantities which all exhibit rearranged Schiff base ligands and which all bear electron-withdrawing substituents on the salicylaldehyde. These three compounds, (**10**) - (**12**), show rearranged Schiff base ligands which encapsulate Mn(III) centers in the two different modes, forming either one or two pockets.

Complex (**10**) shows a similar dimeric structural core as that observed in (**9**), when using 5-nitrosalicylaldehyde together with the asymmetric 322-tetramine, leading to the isolation of [Mn$_2$(5-NO$_2$-Sal$_2$322^{5R})$_2$]·2BuOH. The two Mn(III) ions within the dimeric molecule of complex (**10**) exhibit an octahedral environment. (**10**) crystallizes in triclinic space group P$\bar{1}$ with Z = 2 and the complete crystallographic details can be found in Table A4 in the Appendix. The dimeric Mn(III) compound is assembled from two rearranged Schiff base ligands which chelate the two Mn(III) centers in a head-to-tail fashion in a similar way as was seen within complex (**9**). The ligand rearrangement is analogous to that of the 323-tetramine, and is shown in Scheme 6, leading to the formation of 5-NO$_2$-Sal$_2$322^{5R}, and the establishment of two pockets to incorporate the Mn(III) ions as depicted in Scheme 5. In contrast to complex (**9**), the dimeric unit of (**10**) crystallizes as a neutral entity with two molecules of 2-butanol within the crystal lattice, leading to a molecular formula of [Mn$_2$(5-NO$_2$-Sal$_2$322^{5R})$_2$]·2BuOH (**10**), the structure of which is depicted in Fig. 9.

Even though the backbone of complex (**10**) is reduced by one carbon atom from the 323-tetramine used in complex (**9**), to the 322-tetramine ligand, the observed distance between the two Mn(III) centers is elongated from 6.58 Å observed within (**9**) to 7.94 Å within (**10**) (see Table 7). Both Mn(III) centers, Mn1 and Mn2, are octahedrally coordinated and exhibit an N_3O_3 donor set, which is provided by the two fully deprotonated rearranged 5-NO$_2$-Sal$_2$322^{5R} Schiff base ligands. The coordination sphere is provided by three phenol oxygens, two imine nitrogens, and one amine nitrogen atom of the 5-membered ring. The three oxygen donors, as well as the three nitrogen donors are arranged in a *mer*-conformation, similar to (**8**) and (**9**). The bond lengths are summarized in Table 5 to allow easier comparison between compounds (**9**) and (**10**).

The two axially positioned Mn-O bond lengths around Mn1, Mn1-O6 and Mn1-O18, and around Mn2, Mn2-O9 and Mn2-O15, are between 1.87 and 1.90 Å, and similar to the Mn-O$_{phen}$ bond lengths of (**8**) and (**9**) (Table 5), while the third Mn-O bond length, Mn1-O1 and Mn2-O10, is elongated by ca. 0.2 Å. The two Mn-N$_{imine}$ bond lengths of each Mn(III) center exhibit less deviation between the two bonds, than observed within compounds (**4**) - (**9**), and are in the range between 2.03 and 2.07 Å, and therefore shorter than the range of 2.10–2.15 Å which is observed for Mn(III) centres in the spin quintet state. The bond lengths of 2.34 Å and 2.35 Å to the amine nitrogen atoms of the central 5-membered ring, Mn1-N3 and Mn2-N10, are, respectively, longer than those observed within (**5**) (2.29 Å) and (**9**) (2.31 Å), but not as long, as within (**10**) (2.49 Å).

By switching from 5-nitrosalicylaldehyde to 3,5-dibromosalicylaldehyde we isolated a second dimer with a ligand rearrangement similar to that observed in complex (**10**) (Fig. 10), which gave crystals of [Mn$_2$(3,5-diBr-Sal$_2$322^{5R})(3,5-diBr-Sal)$_3$]·0.7EtOH·2.61MeCN complex (**11**) in very low yield. Complex (**11**) crystallizes in the monoclinic space group $P2_1/c$ with Z = 4 as a dimeric Mn(III) compound but with quite a different arrangement to that observed in (**10**). Both well-separated Mn (III) centers within the dimeric molecule exhibit an octahedral environment, but while Mn1 has an N_2O_4 ligand donor set, Mn2 has an NO_5 one, Fig. 10. The complete crystallographic details for compound (**11**) can be found in Table A5 in the Appendix.

In this case only one fully deprotonated rearranged ligand, 3,5-diBr-Sal$_2$322^{5R}, chelates the two Mn(III) centers in the 2-pocket-mode (Scheme 5), while the remaining vacancies in the coordination sphere are filled by unreacted but deprotonated 3,5-dibromosalicylaldehyde. The bulky bromo substituent in the 3-position of the salicylaldehyde within complex (**11**) could be responsible for prevention of the coordination of a second rearranged Schiff base ligand in a similar way as observed within (**9**) and (**10**) which only have one substituent in the 5-position of the salicylaldehyde. The dimeric complex crystallizes with 2.6 molecules of acetonitrile and 0.7 molecules of ethanol within the crystal lattice, leading to a molecular formula of [Mn$_2$(3,5-diBr-Sal$_2$322^{5R})(3,5-diBr-Sal)$_3$]•2.6MeCN•0.7EtOH.

Table 6
Mn-donor bond lengths in complex (**11**) (in Å). L4 = 3,5-diBr-Sal$_2$322^{5R}

	Mn1		Mn2		
L4 Mn-O_{phen}	Mn1-O3	1.915(4)	L4 Mn-O_{phen}	Mn2-O5	1.872(5)
	Mn1-O4	1.883(4)	L4 Mn-N_{imine}	Mn2-N4	2.027(5)
L4 Mn-N_{imine}	Mn1-N1	2.029(5)	sal Mn-O_{phen}	Mn2-O6	1.894(5)
L4 Mn-N_{amine}	Mn1-N2	2.314(4)		Mn2-O8	1.915(5)
sal Mn-O_{phen}	Mn1-O1	1.921(4)	sal Mn-O_{ald}	Mn2-O7	2.228(5)
sal Mn-O_{ald}	Mn1-O2	2.234(4)		Mn2-O9	2.190(4)

Table 7
Mn-Mn distances observed within (**9**) – (**12**) (in Å).

	Complex (**11**)	Complex (**9**)	Complex (**10**)	Complex (**12**)
Mn-Mn	6.85	6.58	7.94	7.04; 7.12

The structure of (**11**) is shown in Fig. 10 and exhibits a distance between the two Mn(III) centers of 6.85 Å (Table 6). Both Mn(III) centers are octahedrally coordinated; Mn1 exhibits an N_2O_4 donor set, while Mn2 displays an NO_5 donor set. The difference in the ligand environment is based on the coordination mode of the Schiff base ligand.

Compounds (**9**) - (**11**) clearly exhibit long Mn-Mn distances, see Table 7, which suggests that it might be possible to incorporate additional ions in the center of the molecule. This was achieved in the final compound (**12**) which incorporates an additional sodium ion in the center of the dimeric Mn(III) unit, leading to a Mn-Na-Mn arrangement, see Fig. 11 to give [Mn_2Na(3-NO_2,5-OMe-Sal$_2$322^{5R})$_2$]ClO_4·0.5MeCN. Complex (**12**) crystallizes in the monoclinic space group $P2_1$ with two unique trimers in the crystal lattice, Z = 2. The complete crystallographic details for compound (**12**) can be found in Table A5 in the Appendix. All Mn(III) centers within (**12**) are octahedrally coordinated by an N_3O_3 donor set, while the central sodium ion is 8-coordinated by eight oxygen atoms leading to a distorted triangular dodecahedral environment. Only the trimer around Mn1 is depicted as representative for both isostructural trimers in Fig. 11, the bond lengths are provided for both crystallographically unique trimers, Table 8.

The structure consists of two rearranged Schiff base ligands which are based on the rearranged 322-tetramine backbone (as depicted in Scheme 6) in combination with 3-nitro-5-methoxy-salicylaldehyde. In contrast to the previous dimeric structures, (**9**) - (**11**), which exhibit the two Schiff base ligands in a head-to-tail fashion forming two pockets, the Mn(III) centers of complex (**12**) are chelated by a fully deprotonated Schiff base ligand, 3-NO_2,5-OMe-Sal$_2$322^{5R}, in the one-pocket mode, Scheme 5, which is similar to the mononuclear structure of (**5**). This mode allows the incorporation of an additional sodium ion, which is coordinated by four phenol oxygen atoms and four oxygen atoms provided by the nitro substituents of the Schiff base ligand, see Fig. 11. The integration of the central sodium ion, requires an additional anion in the crystal lattice for charge balance, which is provided by one perchlorate anion per trimeric molecule. Additionally, half of a molecule of acetonitrile crystallizes within the unit cell.

The observed distance between the two Mn(III) centers, Mn1 and Mn2, is 7.04 Å (7.12 Å for Mn3-Mn4), with 3.55 Å between Mn1/2 and Na1 (3.58 Å for Mn3/4 and Na2). The angle between the three metal centers, Mn1-Na1-Mn2 is 169.68° (168.47° for Mn3-Na2-Mn4), leading to an almost linear arrangement. All Mn(III) centers, Mn1 and Mn2, as

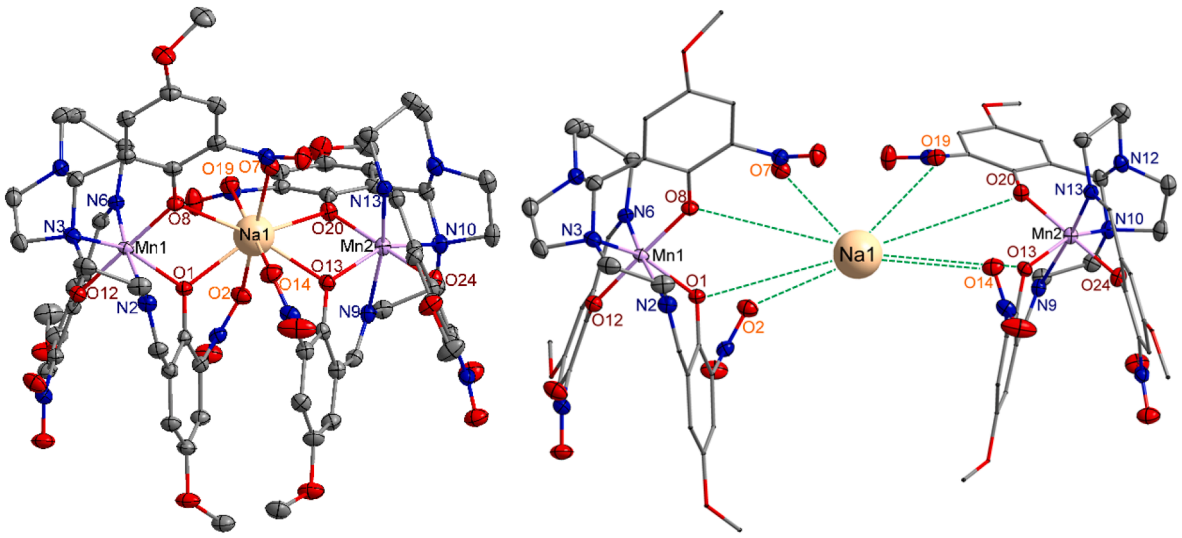

Fig. 11. Molecular structure of (**12**) (left) and schematic built-up of complex (**12**) (right) (perchlorate anions, solvents and H atoms omitted for clarity).

Table 8
Comparison of the Mn-donor bond lengths of the two unique trimers of complex (**12**) (in Å).

	Mn1		Mn2		Mn3		Mn4	
Mn-O_{phen}	Mn1-O12	1.865	Mn2-O24	1.864	Mn3-O36	1.855	Mn4-O48	1.869
	Mn1-O8	1.874	Mn2-O20	1.893	Mn3-O32	1.890	Mn4-O44	1.871
	Mn1-O1	2.131	Mn2-O13	2.117	Mn3-O25	2.078	Mn4-O37	2.133
Mn-N_{imine}	Mn-N2	2.143	Mn2-N9	2.182	Mn3-N20	2.109	Mn4-N27	2.090
	Mn-N6	2.077	Mn2-N13	2.100	Mn3-N16	2.197	Mn4-N23	2.151
Mn-N_{amine}	Mn-N3	2.327	Mn2-N10	2.316	Mn3-N17	2.295	Mn4-N24	2.330

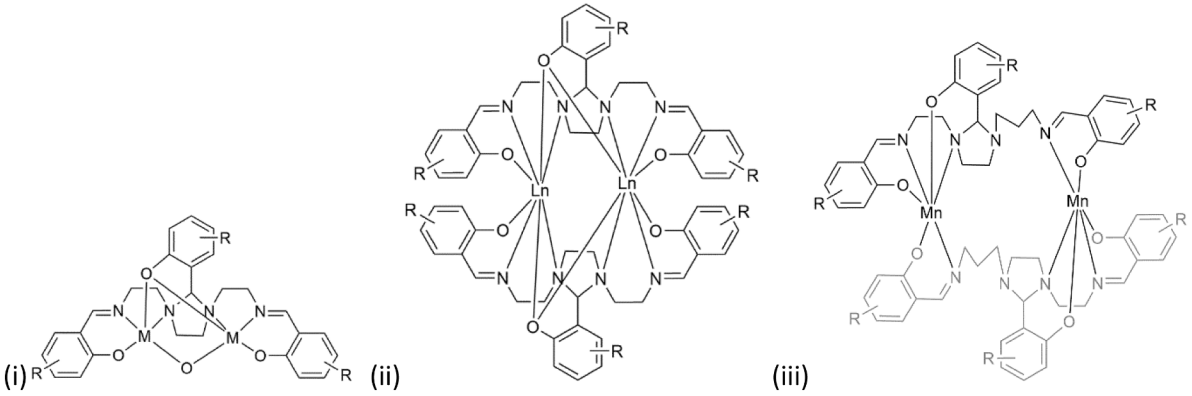

Scheme 7. (i) Binding mode observed for $Sal_2222(5R)$-type ligands coordinated to transition metals, (ii) for dinuclear Ln complexes and (iii) observed for complexes (**9**) - (**12**).

well as Mn3 and Mn4, respectively, are octahedrally coordinated and exhibit an N_3O_3 donor set, which is provided by each rearranged and fully deprotonated Schiff base ligand. The coordination sphere is therefore provided by three phenol oxygens, two imine nitrogens, and one amine nitrogen atom of the 5-membered ring. The three oxygen donors, as well as the three nitrogen donors are arranged in a *mer*-conformation, as seen before. The bond lengths are summarized in Table 8.

In both trimers are two axially positioned Mn-O_{phen} bond lengths, which are in the shorter range between 1.86 and 1.89 Å, similar to the Mn-O_{phen} bond lengths within (**10**), while the third Mn-O_{phen} bond length, (Mn1-O1, Mn2-O13, Mn3-O25 and Mn4-O37), is elongated and in the range between 2.08 and 2.13 Å. The Mn-N_{imine} bond lengths vary between 2.08 and 2.20 Å, while the bond lengths of 2.30–2.33 Å to the amine nitrogen atoms of the 5-membered ring (Mn1-N3, Mn2-N10, Mn3-N17, Mn4-N24), are in a similar range to those observed within (**5**) (2.29 Å) and (**9**) (2.31 Å). The inclusion of a sodium ion in the inter-manganese pocket of (**12**) and the observation of protonation of a separate pocket in the assembly of complex (**9**) indicates the possibilities of inclusion of more biologically relevant guests such as Ca^{2+}, which plays a critical role in the water oxidation center of photosystemII.

4. Comparison of the various binding modes

Since the first report in 1977 of 5-membered ring-closure rearrangement of a Schiff base ligand coordinated to a transition ion, in that case formation of a dinuclear Fe(III) complex [97], the effect has been well documented in complexes with both transition metal ions, lanthanides and combinations of both. Transition metal complexes with R-$Sal_2222(5R)$-type ligands lead, in the majority of cases, to the formation of a dimeric structure where the two metal ions are incorporated each into one of the two pockets offered by the phenolate oxygen, imine nitrogen and amine nitrogen donors, Scheme 7. In this mode the phenolate oxygen of the central salicyl-unit forms a μ_2-bridge between the two metal centers forming a dimeric complex. This type of coordination motif has been observed for the dimers of vanadium [98–101], iron [97,102–104], manganese [105], cobalt [89,106–110], nickel [111–118], copper [119–128] and zinc [129–136]. In addition there are some complexes with higher nuclearities which arise by providing additional ligands that can replace the second μ_2-phenoxo-bridge, leading to higher nuclearity clusters, e.g. Ni_4, Cu_4 and Zn_4, [111,136–142] Ni_5 and Cu_5 [113,123], Cu_4Na [143], Ni_4Cu [144], Ni_6 [145], Zn_2Ln [146,147], or even 3D networks [148] while keeping the same dimeric motif as building unit.

A trend has been observed for dimeric lanthanide complexes, where the requirement for a higher coordination number is met be inclusion of two rearranged Schiff base ligands, each coordinated to both metal ions, Scheme 7, leading to 8-coordinated lanthanide centers [86,149–157]. Each lanthanide ion is chelated into two N_2O_2-pockets where the central phenolate oxygen bridges between the two metal centers.

In contrast to both reported coordination modes in the literature the mode of assembly for compounds (**9**) - (**12**) is new, Scheme 7. While all the literature compounds are symmetrically encapsulated into the two equal pockets, the asymmetry of the 322 backbone might be the reason that in the case of (**9**) - (**12**) one pocket is preferred over the other to incorporate a Mn(III) center leaving one nitrogen atom of the enclosed 5-membered ring uncoordinated.

5. Conclusion

Redox cycling in manganese complexes and biological sites is well established and underpins many of the applications of this versatile element. Of equal importance is the role of magnetic anisotropy in promoting single molecule magnetism in numerous clusters that have been expertly studied over the last three decades. Less well-explored is the rich electronic diversity within the trivalent form of the ion, which can assume a compressed or elongated Jahn-Teller effect, with associated differences in anisotropy, and also ready access to more than one arrangement of spins with the right donor sphere. We have tried here to examine the prevalence of both effects – choice of Jahn-Teller direction and ability to undergo spin triplet-quintet switching – in three different geometric frameworks: R-Sal_2323, R-Sal_2333 and R-Sal_2322. We have demonstrated a clear preference for mononuclear coordination with rare axial compression in the R-Sal_2323 and R-Sal_2333 frameworks, in contrast to the strong tendency for ligand rearrangement and dimer formation with the shorter and less symmetric R-Sal_2322 sphere. We have also shown that although thermal spin state switching is possible in one of the axially-compressed frameworks, that with R-Sal_2323, it has not yet been observed with alternative frameworks which are also compressed, *i.e.* R-Sal_2333, thereby demonstrating that axial compression is not the only factor at play. Finally, the ease with which the mononuclear assembly mode is abandoned when the alkyl connectivity is reduced by just one carbon augurs well for other types of application, including biomimicry and perhaps small molecule activation by Mn complexes with the shorter ligand type. Despite its simplicity, the versatility of the hexadentate ligand type employed here in the binding

and electronic tuning of Mn^{3+} should not be underestimated. These results illustrate the depth of electronic structure that is achievable within just one valence state of a fascinating and versatile element by judicious choice of coordination framework, and our efforts to uncover new phenomena and associated applications with such assemblies continues.

6. Materials and methods

6.1. Materials and physical measurements

All chemicals and solvents if not otherwise mentioned were purchased from chemical companies and were reagent grade. They were used without further purification or drying. All reactions were carried out under ambient conditions. All measurements were carried out on powdered samples of the respective polycrystalline compound which in some cases were fitted with partial solvation according to CHN data on the bulk sample. Elemental analysis (C, H and N) were performed using a Perkin Elmer Vario EL instrument. A Bruker Alpha PlatinumATIR spectrometer was used to record the infrared spectra, and mass spectra were recorded on a Waters 2695 Separations Module Electrospray Spectrometer.

7. Synthesis and characterization

7.1. Compounds (1) – (3)

Complex (**1**) - [Mn(5-F-Sal$_2$323)]CF_3SO_3: 5-Fluoro-2-hydroxysalicylaldehyde (280 mg, 2.0 mmol) was dissolved in a 1:1 solution of MeCN:EtOH (25 mL), and 1,2-bis(3-aminopropylamino)ethane (174 mg, 1.0 mmol) was added. This yellow ligand solution was stirred for 10 min before $MnCl_2$•$4H_2O$ (198 mg, 1.0 mmol) was added together with lithium trifluoromethanesulfonate (156 mg, 1.0 mmol) for salt metathesis. Upon addition of the metal salt, the solution turned brown, and was stirred for one hour. The solution was then filtered, left standing for crystallization, yielding suitable single crystals. Elemental analysis for (**1**): Calculated for $C_{23}H_{26}F_5MnN_4O_5S{\cdot}H_2O$; C = 43.27, H = 4.42, N = 8.77; found: C = 42.92, H = 4.05, N = 9.18.

Complex (**2**) - [Mn(5-F-Sal$_2$323)]ClO_4: The synthesis was done in a similar way as for (**1**), using directly $Mn(ClO_4)_2$•$6H_2O$ (362 mg, 1.0 mmol). Elemental analysis for (**2**): Calculated for $C_{22}H_{26}ClF_2MnN_4O_6$; C = 46.29, H = 4.59, N = 9.81; found: C = 45.96, H = 4.57, N = 9.57.

Complex (**3**) - [Mn(5-F-Sal$_2$323)]NO_3: The synthesis was done in a similar way as for (**1**), using directly $Mn(NO_3)_2$•$4H_2O$ (251 mg, 1.0 mmol). Elemental analysis for (**3**): Calculated for $C_{22}H_{26}F_2MnN_5O_5{\cdot}0.15H_2O$; C = 49.29, H = 4.94, N = 13.06; found: C = 49.06, H = 4.70, N = 13.03.

7.2. Compounds (4) – (8)

Complex (**4**) - [Mn(3-OEt-Sal$_2$333)]BF_4: In a 100 mL beaker, N,N'-bis (3-aminopropyl)-1,3-propan-diamine (0.204 mL, 1 mmol), was dissolved in 1:1 EtOH/MeCN,(25 mL) then 3-ethoxysalicylaldehyde (0.333 g, 2 mmol) was added forming a yellow colored solution which was stirred for 15 min. $MnCl_2$•$4H_2O$ (198 mg, 1.0 mmol) was added to the mixture, and a color change from yellow to deep purple was observed. The reaction mixture was stirred for 15 min at room temperature. Ammonium tetrafluoroborate, NH_4BF_4, (0.1048 g, 1 mmol) was then added to the reaction beaker and stirred well for 45 min. The mixture was then gravity filtered and the solvent was allowed to evaporate slowly at room temperature. After 48 h dark black crystals were obtained. FT-IR (cm^{-1}): 2982, 1610, 1446, 1295, 1282, 1055, 893, 848, 737. Mass spec $[C_{27}H_{38}N_4O_4Mn]^+$: 538.56 M^+ (expected: 537.56).

Complex (**5**) - [Mn(3,5-diOMe-Sal$_2$333)]BF_4•$0.5C_3H_8O$: In a 100 mL beaker, N,N'-bis(3-aminopropyl)-1,3-propan-diamine (0.102 mL, 0.5 mmol), was dissolved in 1:1 EtOH/MeCN (15 mL) before addition of solid 4,6-dimethoxysalicylaldehyde (0.182 g, 1.0 mmol) forming a yellow colored solution which was stirred for 15 min. Solid $MnCl_2$•$4H_2O$ (0.099 g, 0.5 mmol) was added causing a color change from yellow to deep purple and the reaction mixture was stirred for 30 min at room temperature. Solid ammonium tetrafluoroborate NH_4BF_4, (0.052 g, 0.5 mmol) was then added to the reaction beaker and stirred well for 45 min. The mixture was then gravity filtered and the solvent was allowed to evaporate slowly at room temperature. After 48 h dark black crystals were obtained. Mass spec $[C_{27}H_{38}N_4O_6Mn]^+$: 570.50 M^+ (expected: 569.56). FT-IR (cm^{-1}): 3270, 1595, 1549, 1417, 1379, 1204, 1122, 1049, 816, 789, 657.

Complex (**6**) - [Mn(5-F-Sal$_2$333)]BPh_4: In a 100 mL beaker, N,N'-bis (3-aminopropyl)-1,3-propandiamine (0.102 mL, 0.5 mmol), was dissolved in 1:1 EtOH/MeCN (15 mL). 5-Fluorosalicylaldehyde (0.140 g, 1.0 mmol) was added forming a yellow colored solution which was stirred for 15 min. $MnCl_2$•$4H_2O$ (0.099 g, 0.5 mmol) was added to the mixture and a color change from yellow to deep purple was observed. The reaction mixture was stirred for 30 min at room temperature. Solid sodium tetraphenylborate, $NaBPh_4$, (0.171 g, 0.5 mmol) was then added to the reaction beaker and stirred well for 45 min. The mixture was then gravity filtered and the solvent was allowed to evaporate slowly at room temperature. After 48 h dark black crystals were obtained. Mass spec.: $[C_{23}H_{28}N_4O_2F_2Mn]^+$: 484.11 M^+ (expected: 485.44).

FT-IR (cm^{-1}): 3050, 1623, 1553, 1468, 1261, 1148, 816, 733, 703, 610.

Complex (**7**) - [Mn(5-NO_2-Sal$_2$333)]BPh_4: In a 100 mL beaker, N,N'-bis (3-aminopropyl)-1,3-propandiamine (0.102 mL, 0.5 mmol), was dissolved in 1:1 ethanol/acetonitrile (15 mL). 5-Nitrosalicylaldehyde (0.167 g, 1.0 mmol,) was added forming a yellow colored solution which was then stirred for 15 min. $MnCl_2$•$4H_2O$ (0.099 g, 0.5 mmol) was added to the mixture and a color change from yellow to deep purple was observed and the reaction mixture was stirred for 30 min at room temperature. Sodium tetraphenylborate (0.171 g, 0.5 mmol) was then added to the reaction beaker and stirred well for 45 min. The mixture was then gravity filtered and the solvent was allowed to evaporate slowly at room temperature. After 48 h dark black crystals were obtained.

Complex (**8**) – [Mn(3-OMe,5-NO_2-Sal$_2$333^{6R})]·0.07MeOH·0.93MeCN: In a 100 mL beaker, N,N'-bis(3-aminopropyl)-1,3-propandiamine (0.102 mL, 0.5 mmol), was dissolved in 1:1 EtOH/MeCN (15 mL). 3-Methoxy-5-nitrosalicylaldehyde (0.197 g, 1.0 mmol) was added forming a yellow colored solution which was stirred for 15 min. Mn$(ClO_4)_2$•$6H_2O$ (181 mg, 0.5 mmol) was added causing a color change from yellow to deep purple and the reaction mixture was stirred for 30 min at room temperature. The mixture was then gravity filtered and the solvent was allowed to evaporate slowly at room temperature. After one week, dark black crystals were obtained in very small yield.

7.3. Compounds (9) – (12)

Complex (**9**) - $[Mn_2$(5-Cl-Sal$_2$323^{H5R})$_2]$$(ClO_4)_2$·1.85EtOH·0.33MeCN: In a typical synthesis attempt 5-chloro-2-hydroxysalicylaldehyde (78 mg, 0.5 mmol) was dissolved in a 1:1 solution of MeCN:EtOH (25 mL), and 1,2-bis(3-aminopropylamino)ethane (44 mg, 0.25 mmol) was added. This yellow ligand solution was stirred for 10 min before addition of solid $Mn(ClO_4)_2$•$6H_2O$ (90 mg, 0.25 mmol), leading to a color change

to brown. The reaction mixture was stirred for an hour, filtered and left to stand for crystallization. The resulting crystalline product was observed in very small quantities and was analysed by single crystal diffraction.

Complex (**10**) - [Mn_2(5-NO_2-sal_2322^{5R})$_2$]·2BuOH: In a typical procedure 5-nitro-2-hydroxysalicylaldehyde (83 mg, 0.5 mmol) was dissolved in a 1:1 solution of MeCN:EtOH (25 mL), and N-(2-aminoethyl)-N'-(3-aminopropyl)ethylenediamine tetrahydrochloride (49 mg, 0.25 mmol) was added. Ground sodium hydroxide (0.04 g, 1.00 mmol) was added to neutralize the amine hydrochloride and the pale orange solution was stirred for 10 min. This yellow ligand solution was stirred for 10 min before $Mn(ClO_4)_2$•$6H_2O$ (90 mg, 0.25 mmol) was added, leading to a color change to brown. The reaction mixture was stirred for an hour, then filtered and left standing for crystallization. The resulting crystalline product was recovered only in very small quantities and was analysed by single crystal diffraction.

Complex (**11**) - [$Mn_2$3,5-diBr-Sal_2322^{5R})(3,5-diBr-Sal)$_3$]·0.7EtOH·2.61MeCN••: 322-tetrahydrochloride (0.153 g, 0.5 mmol) was dissolved in ethanol (20 mL) in a 100 mL beaker. Ground sodium hydroxide (0.08 g, 2.00 mmol) was added to neutralize the amine hydrochloride and the pale orange solution was stirred for 10 min. The solution was then filtered into a 100 mL beaker. 3,5-dibromosalicylaldehyde (1 mmol, 0.28 g) was added and a yellow solution was observed. The solution was stirred for 45 min. $Mn(NO_3)$ $4H_2O$ (0.5 mmol, 0.126 g) was added to a 100 mL sample vial containing MeCN (20 mL). The ethanol ligand solution was then filtered into the acetonitrile metal solution, a black color was observed. The mixture was then stirred for 45 min and covered in parafilm. After one week, small black crystals were observed. The product was analyzed by X-ray crystallography.

Complex (**12**) – [Mn_2Na(3-NO_2,5-OMe-Sal_2322^{5R})$_2$]ClO_4·0.5MeCN: In a typical synthesis 322-tetrahydrochloride (0.153 g, 0.5 mmol) was dissolved in ethanol (20 mL) in a 100 mL beaker. Ground sodium hydroxide (0.08 g, 2.00 mmol) was added to neutralize the amine tetrachloride. The pale orange solution was stirred for 10 min and then filtered. 3-Nitro 5-methoxysalicylaldehyde (0.197 g, 1.0 mmol) was added, and the mixture was stirred for 45 min to complete the Schiff base reaction. $Mn(NO_3)$·$4H_2O$ (0.5 mmol, 0.126 g) was dissolved in MeCN (20 mL). The ethanolic Schiff base solution was then filtered into the metal-containing acetonitrile solution, and a color change to black was observed. The mixture was then stirred for 45 min, filtered and covered with parafilm to allow for slow evaporation. Small black crystals were obtained in very low yield which were analysed by single crystal diffraction.

7.4. Single-Crystal X-ray structure determination

Suitable single crystals of complexes (**1**) to (**12**) were mounted on Oxford Diffraction Supernova A diffractometer fitted with an Atlas detector; datasets were measured using monochromatic Cu-Kα radiation or Mo-*K*α radiation and corrected for absorption [158]. The temperatures were controlled with an Oxford Instruments' Cryojet. Structures were solved by direct methods (SHELXS) and refined with full-matrix least-squared procedures based on F^2, using SHELXL-1997 or −2016 [159]. Non-hydrogen atoms were refined with independent anisotropic displacement parameters, organic H-atoms (*i.e.*, bonded to C) were placed in idealized positions, while the coordinates of H-atoms bonded to O were generally refined with their O—H distance restrained to 0.84 Å; details are described in the cif for each structure. In general, if disorder had to be modelled, the sum of the site occupation factors was con-or restrained to be 1. Selected crystallographic data and structure refinements are summarized in Tables A1–A3 (see Appendices). CCDC 2073371–2073379 contain the supplementary crystallographic data for complexes (**1**)-(**12**). These data can be obtained free of charge via http://www.ccdc.cam.ac.uk/conts/retrieving.html, or from the Cambridge Crystallographic Data Centre, 12 Union Road, Cambridge CB2 1EZ, UK; fax: (+44) 1223–336-033; or e-mail: deposit@ccdc.cam.ac.uk.

Table A1
Crystallographic details for complexes (**1**) – (**2**).

Compound	(**1**) [100 K]	(**2**) [100 K]	(**2**) [293 K]
sample code	mor845	mor828	mor827
Empirical formula	$C_{23}H_{26}N_4O_5F_5SMn$	$C_{22}H_{26}N_4O_6F_2ClMn$	$C_{22}H_{26}N_4O_6F_2ClMn$
Formula weight	620.48	570.86	570.86
Temperature (K)	100(2)	100(2)	293(2)
Radiation	Cu-Kα	Mo-Kα	Mo-Kα
Crystal system	monoclinic	Triclinic	Triclinic
Space group	*P*2/*c*	*P*-1 (#2)	*P*-1 (#2)
Crystal size (mm)	0.433 × 0.295 × 0.187	0.325 × 0.224 × 0.209	0.305 × 0.231 × 0.187
a (Å)	18.1539(1)	7.37132(7)	7.49774(6)
b (Å)	8.10550(5)	10.5108(2)	10.67870(8)
c (Å)	17.5509(1)	15.9740(2)	15.9789(1)
α (°)	90	85.7873(9)	86.9064(6)
β (°)	92.9199(6)	78.2732(7)	80.0555(6)
γ (°)	90	79.0920(9)	79.4049(6)
V (Å^3)	2579.20(3)	1189.13(3)	1238.337(16)
Z	4	2	2
d_{calc} (g cm^{-3})	1.598	1.594	1.531
μ (mm^{-1})	5.638	0.731	0.702
F(0 0 0)	1272	588	588
Limiting indices	h = ±22, k = ±10, I = ±22	h = ±11, k = ±16, I = ±23	h = ±9, K = ±14, I = ±21
Reflect. coll./uniq.	26957/5403	75782/8527	64759/6134
R(int)	0.0264	0.0288	0.02
Complete to Θ (%)	99.4	99.6	99.7
Data/restr./param.	5403/0/353	8527/0/333	6134/0/346
GooF on F^2	1.046	1.045	1.06
Final R indices [I > 2σ (I)][a]	R_1 = 0.0273, wR_2 = 0.0718	R_1 = 0.0290, wR_2 = 0.0767	R_1 = 0.0332, wR_2 = 0.0938
R indices (all data)	R_1 = 0.0279, wR_2 = 0.0724	R_1 = 0.0323, wR_2 = 0.0792	R_1 = 0.0353, wR_2 = 0.0958
Largest diff. peak/hole (e·Å^{-3})	0.260 and –0.461	0.717 and –0.474	0.346 and –0.410
CSD no.	2,085,168	2,085,167	2,085,813

Table A2
Crystallographic details for complexes (**3**)–(**5**).

Compound	(**3**)	(**4**)	(**5**)
sample code	mor826	mor918	mor916sqz
Empirical formula	$C_{22}H_{26}N_5O_5F_2Mn$	$C_{27}H_{38}BN_4O_4F_4Mn$	$C_{57}H_{84}B_2N_8O_{13}F_8Mn_2$
Formula weight	533.42	624.36	1372.82
Temperature (K)	293(2)	100(2)	100(2)
Radiation	Mo-Kα	Cu-Kα	Cu-Kα
Crystal system	orthorhombic	Monoclinic	Monoclinic
Space group	Pccn (#56)	$P2_1/c$ (#14)	$P2_1/c$ (#14)
Crystal size (mm)	0.548 × 0.380 × 0.312	0.213 × 0.051 × 0.044	0.252 × 0.047 × 0.024
a (Å)	8.4080(2)	11.6439(2)	7.3961(2)
b (Å)	16.1752(4)	20.0555(2)	26.3241(5)
c (Å)	17.6948(4)	13.3498(2)	16.1692(4)
α (°)	90	90	90
β (°)	90	111.873(2)	101.116(3)
γ (°)	90	90	90
V (Å^3)	2406.51(10)	2893.08(7)	3089.01(13)
Z	4	4	2
d_{calc} (g cm^{-3})	1.472	1.433	1.476
μ (mm^{-1})	0.607	4.285	4.13
F(0 0 0)	1104	1304	1436
Limiting indices	h=±10, k=±19, I=±21	h = ±14, k = ±25, l = ±16	h = ±9, k = ±32, l = ±20
Reflect. coll./uniq.	17823/2123	30663/6074	29081/6448
R(int)	0.0194	0.0255	0.0468
Complete to Θ (%)	99.6	98.9	98.8
Data/restr./param.	2123/0/164	6074/0/372	6448/0/392
GooF on F^2	1.048	1.096	1.123
Final R indices [I > 2 σ (I)][a]	R_1 = 0.0389, wR_2 = 0.1039	R_1 = 0.0307, wR_2 = 0.0806	R_1 = 0.0813, wR_2 = 0.2108
R indices (all data)	R_1 = 0.0424, wR_2 = 0.1085	R_1 = 0.0325, wR_2 = 0.0818	R_1 = 0.0857, wR_2 = 0.2129
Largest diff. peak/hole (e·Å^{-3})	0.341 and –0.425	0.691 and –0.546	1.429 and –1.236
CSD no.	2,085,166	2,073,373	2,073,371

Table A3
Crystallographic details for complexes (**6**) – (**8**).

Compound	(**6**)	(**7**)	(**8**)
sample code	mor917	mor1416	mor1263
Empirical formula	$C_{47}H_{48}BN_4O_2F_2Mn$	$C_{47}H_{48}BN_6O_6Mn$	$C_{34.93}H_{39.07}N_{7.93}O_{12.07}Mn$
Formula weight	804.64	858.66	818.05
Temperature (K)	100(2)	100(2)	100(2)
Radiation	Mp-Kα	Cu-Kα	Mo-Kα
Crystal system	Triclinic	Orthorhombic	Triclinic
Space group	*P*-1 (#2)	*Pna*2$_1$ (#33)	*P*-1 (#2)
Crystal size (mm)	0.328 × 0.204 × 0.173	0.123 × 0.098 × 0.079	0.296 × 0.227 × 0.191
a (Å)	10.63915(9)	21.4944(2)	10.9429(1)
b (Å)	13.9972(2)	9.9167(1)	12.1194(1)
c (Å)	14.9635(1)	19.6521(2)	13.4433(2)
α (°)	103.8319(7)	90	85.5622(7)
β (°)	93.6862(7)	90	87.9383(8)
γ (°)	109.1681(8)	90	88.6100(7)
V (Å^3)	2018.84(4)	4188.91(7)	1775.96(3)
Z	2	4	2
d_{calc} (g cm^{-3})	1.324	1.362	1.53
μ (mm^{-1})	0.381	3.033	0.45
F(0 0 0)	844	1800	851.4
Limiting indices	h = ±15, k = ±20, l = ±21	h = ±27, k = ±12, l = ±24	h = ±16, k=±18, l = ±20
Reflect. coll./uniq.	87030/12218	45262/7974	67704/12563
R(int)	0.048	0.048	0.0269
Complete to Θ (%)	99.1	100.0	99.8
Data/restr./param.	12,218/0/514	7974/1/580	12,563/0/530
GooF on F^2	1.029	1.037	1.086
Final R indices [I > 2 σ (I)][a]	R_1 = 0.0355, wR_2 = 0.0873	R_1 = 0.0369, wR_2 = 0.0904	R_1 = 0.0354, wR_2 = 0.0866
R indices (all data)	R_1 = 0.0402, wR_2 = 0.0904	R_1 = 0.0418, wR_2 = 0.0940	R_1 = 0.0449, wR_2 = 0.0929
Largest diff. peak/hole (e·Å^{-3})	0.511 and –0.546	0.435 and –0.578	0.492 and –0.295
CSD no.	2,073,372	2,073,378	2,073,377

Table A4
Crystallographic details for complexes (**9**) – (**10**).

Compound	(**9**)	(**10**)
sample code	mor1201	mor954sqz
Empirical formula	$C_{62.36}H_{70.08}N_{8.33}O_{15.85}Cl_8Mn_2$	$C_{64}H_{72}N_{14}O_{20}Mn_2$
Formula weight	1583.43	1467.24
Temperature (K)	100(2)	100(2)
Radiation	Cu-Kα	Mo-Kα
Crystal system	Trigonal	Triclinic
Space group	*R*-3 (#148)	*P*-1 (#2)
Crystal size (mm)	0.306 × 0.134 × 0.108	0.303 × 0.221 × 0.062
a (Å)	39.1897(4)	14.9797(3)
b (Å)	39.1897(4)	16.4885(3)
c (Å)	11.8314(1)	17.3571(3)
α (°)	90	64.832(2)
β (°)	90	67.154(2)
γ (°)	120	89.160(2)
V (Å^3)	15736.6(3)	3517.04(11)
Z	9	2
d_{calc} (g cm^{-3})	1.504	1.385
μ (mm^{-1})	6.35	0.44
F(0 0 0)	7338.4	1528
Limiting indices	h = ±49, k = ±45, l = ±14	h = ±18, k = ±20, l = ±21
Reflect. coll./uniq.	33606/7316	63796/14388
R(int)	0.0319	0.0326
Complete to Θ (%)	100.0	99.8
Data/restr./param.	7316/0/490	14,388/0/858
GooF on F^2	1.036	1.057
Final R indices [I > 2 σ (I)][a]	R_1 = 0.0326, wR_2 = 0.0873	R_1 = 0.0688, wR_2 = 0.2071
R indices (all data)	R_1 = 0.0362, wR_2 = 0.0904	R_1 = 0.0788, wR_2 = 0.2164
Largest diff. peak/hole (e·Å^{-3})	0.957 and –0.419	1.756 and –1.148
CSD no.	2,073,376	2,073,374

Table A5
Crystallographic details for complexes (**11**) – (**12**).

Compound	(**11**)	(**12**)
sample code	mor1057	mor1483
Empirical formula	$C_{55.6}H_{44}N_{6.6}O_{9.7}Mn_2Br_{12}$	$C_{126}H_{131}N_{29}O_{56}Na_2Cl_2Mn_4$
Formula weight	2029.12	3284.23
Temperature (K)	100(2)	100(2)
Radiation	Cu-Kα	Cu-Kα
Crystal system	Monoclinic	Monoclinic
Space group	$P2_1/c$ (#14)	$P2_1$ (#4)
Crystal size (mm)	0.251 × 0.244 × 0.084	0.182 × 0.100 × 0.087
a (Å)	22.2808(3)	14.46940(9)
b (Å)	15.0288(2)	27.2519(2)
c (Å)	19.7713(3)	18.0885(1)
α (°)	90	90
β (°)	99.845(2)	107.3156(6)
γ (°)	90	90
V (Å^3)	6523.00(16)	6809.38(8)
Z	4	2
d_{calc} (g cm^{-3})	2.066	1.602
μ (mm^{-1})	12.26	4.306
F(0 0 0)	3887	3388
Limiting indices	h=±27, k=±18, l=±24	h = ±18, k=±33, l = ±22
Reflect. coll./uniq.	39787/13610	139137/27842
R(int)	0.0361	0.0381
Complete to Θ (%)	100.0	100.0
Data/restr./param.	13,610/0/747	27,842/1/2004
GooF on F^2	1.075	1.007
Final R indices [I > 2 σ (I)][a]	R_1 = 0.0563, wR_2 = 0.1327	R_1 = 0.0295, wR_2 = 0.0762
R indices (all data)	R_1 = 0.0625, wR_2 = 0.1371	R_1 = 0.0307, wR_2 = 0.0772
Largest diff. peak/hole (e·Å^{-3})	1.720 and –1.969	0.634 and –0.503
CSD no.	2,073,375	2,073,379

7.5. Magnetic measurements

The magnetic susceptibility measurements were recorded on a Quantum Design SQUID magnetometer MPMS-XL operating between 1.8 and 300 K. DC measurements were performed on polycrystalline samples. Each sample was wrapped in a gelatine capsule and subjected to fields of 0.5 T. Diamagnetic corrections were applied to correct for contribution from the sample holder, and the inherent diamagnetism of the sample was estimated with the use of Pascal's constants.

CRediT authorship contribution statement

Sriram Sundaresan: Investigation, Methodology. **Irina A. Kühne:** Conceptualization, Data curation, Formal analysis, Investigation, Methodology, Project administration, Visualization, Writing – original draft, Writing - review & editing. **Colin Evesson:** Investigation, Methodology. **Michelle M. Harris:** Investigation, Methodology, Formal analysis. **Anthony J. Fitzpatrick:** Investigation, Methodology. **Ahmed Ahmed:** Investigation, Methodology. **Helge Müller-Bunz:** Data curation, Formal analysis, Investigation, Methodology. **Grace G. Morgan:** Conceptualization, Data curation, Funding acquisition, Investigation, Methodology, Project administration, Resources, Supervision, Writing - review & editing.

Declaration of Competing Interest

The authors declare that they have no known competing financial interests or personal relationships that could have appeared to influence the work reported in this paper.

Acknowledgements

We gratefully acknowledge support from the UCD School of Chemistry for technical support and use of facilities.

Funding

We thank Science Foundation Ireland and the Irish Research Council for generous support via SFI Frontiers for the Future Award (SFI 19/FFP/6909 to G.G.M) and a Postdoctoral Fellowship (IRC GOIPD/2016/503 to I.A.K.). We also thank the National University of Ireland for Traveling Scholarships (to M.M.H, A.J.F. and C.E.) and the Cultural Service of the French Embassy in Ireland for a PhD Studentship (to A.J.F.). All authors acknowledge the generous support of University College Dublin, particularly for the award of part studentships/fee waivers to C.E., M.M.H., A.J.F and S.S. Significant funding for a SQUID magnetometer by the Irish Higher Education Authority is also gratefully acknowledged as is financial support from EU COST Actions CA15128 Molecular Spintronics (MOLSPIN), CM1305 Explicit Control over Spin-states in Technology and Biochemistry, (ECOSTBio), and CA15107 Multi-Functional Nano-Carbon Composite Materials Network (MultiComp).

References

[1] Y. Umena, K. Kawakami, J.-R. Shen, N. Kamiya, Crystal structure of oxygen-evolving photosystem II at a resolution of 1.9 Å, Nature 473 (2011) 55–60, https://doi.org/10.1038/nature09913.
[2] H. Dau, C. Limberg, T. Reier, M. Risch, S. Roggan, P. Strasser, The mechanism of water oxidation: from electrolysis via homogeneous to biological catalysis, ChemCatChem 2 (7) (2010) 724–761, https://doi.org/10.1002/cctc.201000126.
[3] V.K. Yachandra, K. Sauer, M.P. Klein, Manganese cluster in photosynthesis: where plants oxidize water to dioxygen, Chem. Rev. 96 (1996) 2927–2950, https://doi.org/10.1021/cr950052k.
[4] J.W. Whittaker, M.M. Whittaker, Active site spectral studies on manganese superoxide dismutase, J. Am. Chem. Soc. 113 (15) (1991) 5528–5540, https://doi.org/10.1021/ja00015a003.
[5] A.-F. Miller, Superoxide dismutases: ancient enzymes and new insights, FEBS Lett. 586 (2012) 585–595, https://doi.org/10.1016/j.febslet.2011.10.048.

[6] A.-F. Miller, Superoxide dismutases: active sites that save, but a protein that kills, Curr. Opin. Chem. Biol. 8 (2) (2004) 162–168, https://doi.org/10.1016/j.cbpa.2004.02.011.

[7] G.M. Edelman, B.A. Cunningham, G.N. Reeke, J.W. Becker, M.J. Waxdal, J. L. Wang, The covalent and three-dimensional structure of concanavalin A, Proc. Natl. Acad. Sci. U.S.A. 69 (9) (1972) 2580–2584, https://doi.org/10.1073/pnas.69.9.2580.

[8] M.D. Sampson, A.D. Nguyen, K.A. Grice, C.E. Moore, A.L. Rheingold, C.P. Kubiak, Manganese catalysts with bulky bipyridine ligands for the electrocatalytic reduction of carbon dioxide: eliminating dimerization and altering catalysis, J. Am. Chem. Soc. 136 (14) (2014) 5460–5471, https://doi.org/10.1021/ja501252f.

[9] Y. Gao, T. Åkermark, J. Liu, L. Sun, B. Åkermark, Nucleophilic attack of hydroxide on a Mn(V) Oxo complex: a model of the O−O Bond formation in the oxygen evolving complex of photosystem II, J. Am. Chem. Soc. 131 (25) (2009) 8726–8727, https://doi.org/10.1021/ja901139r.

[10] C. Mullins, V. Pecoraro, Reflections on small molecule manganese models that seek to mimic photosynthetic water oxidation chemistry, Coord. Chem. Rev. 252 (3-4) (2008) 416–443, https://doi.org/10.1016/j.ccr.2007.07.021.

[11] R. Sessoli, H.L. Tsai, A.R. Schake, S. Wang, J.B. Vincent, K. Folting, D. Gatteschi, G. Christou, D.N. Hendrickson, High-spin molecules: $[Mn_{12}O_{12}(O_2CR)_{16}(H_2O)_4]$, J. Am. Chem. Soc. 115 (5) (1993) 1804–1816, https://doi.org/10.1021/ja00058a027.

[12] G. Christou, D. Gatteschi, D.N. Hendrickson, R. Sessoli, Single-Molecule Magnets, MRS Bull. 25 (11) (2000) 66–71, https://doi.org/10.1557/mrs2000.226.

[13] C.-K. Yang, Y. Yamazaki, A. Aydin, S.M. Haile, Thermodynamic and kinetic assessments of strontium-doped lanthanum manganite perovskites for two-step thermochemical water splitting, J. Mater. Chem. A 2 (33) (2014) 13612–13623, https://doi.org/10.1039/C4TA02694B.

[14] M. Kubicek, A.H. Bork, J.L.M. Rupp, Perovskite oxides – a review on a versatile material class for solar-to-fuel conversion processes, J. Mater. Chem. A. 5 (24) (2017) 11983–12000, https://doi.org/10.1039/C7TA00987A.

[15] T. Cooper, J.R. Scheffe, M.E. Galvez, R. Jacot, G. Patzke, A. Steinfeld, Lanthanum manganite perovskites with Ca/Sr A-site and Al B-site doping as effective oxygen exchange materials for solar thermochemical fuel production, Energy Technol. 3 (11) (2015) 1130–1142, https://doi.org/10.1002/ente.201500226.

[16] Y. Tokura, Critical features of colossal magnetoresistive manganites, Reports Prog. Phys. 69 (3) (2006) 797–851, https://doi.org/10.1088/0034-4885/69/3/R06.

[17] T. Chatterji, G. Jackeli, N. Shannon, in: Colossal Magnetoresistive Manganites, Springer Netherlands, Dordrecht, 2004, pp. 321–382, https://doi.org/10.1007/978-94-015-1244-2_8.

[18] Y. Tokura, Orbital Physics in Transition-Metal Oxides, Science 288 (2000) 462–468, https://doi.org/10.1126/science.288.5465.462.

[19] T. Goto, T. Kimura, G. Lawes, A.P. Ramirez, Y. Tokura, Ferroelectricity and giant magnetocapacitance in perovskite rare-earth manganites, Phys. Rev. Lett. 92 (2004), 257201, https://doi.org/10.1103/PhysRevLett.92.257201.

[20] M. Fiebig, T.h. Lottermoser, D. Fröhlich, A.V. Goltsev, R.V. Pisarev, Observation of coupled magnetic and electric domains, Nature 419 (2002) 818–820, https://doi.org/10.1038/nature01077.

[21] T.C. Stamatatos, D. Foguet-Albiol, S.-C. Lee, C.C. Stoumpos, C.P. Raptopoulou, A. Terzis, W. Wernsdorfer, S.O. Hill, S.P. Perlepes, G. Christou, "Switching On" the properties of single-molecule magnetism in triangular manganese(III) complexes, J. Am. Chem. Soc. 129 (30) (2007) 9484–9499, https://doi.org/10.1021/ja072194p.

[22] J. Cirera, E. Ruiz, S. Alvarez, F. Neese, J. Kortus, How to build molecules with large magnetic anisotropy, Chem. Eur. J. 15 (16) (2009) 4078–4087, https://doi.org/10.1002/chem.v15:1610.1002/chem.200801608.

[23] F. Liedy, J. Eng, R. McNab, R. Inglis, T.J. Penfold, E.K. Brechin, J.O. Johansson, Vibrational coherences in manganese single-molecule magnets after ultrafast photoexcitation, Nat. Chem. 12 (5) (2020) 452–458, https://doi.org/10.1038/s41557-020-0431-6.

[24] P.L.W. Tregenna-Piggott, Origin of compressed Jahn−Teller octahedra in sterically strained manganese(III) complexes, Inorg. Chem. 47 (2) (2008) 448–453, https://doi.org/10.1021/ic700968q.

[25] Q. Scheifele, C. Riplinger, F. Neese, H. Weihe, A.-L. Barra, F. Juranyi, A. Podlesnyak, P.L.W. Tregenna-Piggott, Spectroscopic and theoretical study of a mononuclear manganese(III) complex exhibiting a tetragonally compressed geometry, Inorg. Chem. 47 (2) (2008) 439–447, https://doi.org/10.1021/ic701665u.

[26] J. Krzystek, G.J. Yeagle, J.-H. Park, R.D. Britt, M.W. Meisel, L.-C. Brunel, J. Telser, High-frequency and -Field EPR Spectroscopy of Tris(2,4-pentanedionato) manganese(III): investigation of solid-state versus solution Jahn−Teller effects, Inorg. Chem. 42 (2003) 4610–4618, https://doi.org/10.1021/ic020712l.

[27] C. Mantel, A.K. Hassan, J. Pécaut, A. Deronzier, M.-N. Collomb, C. Duboc-Toia, A high-frequency and high-field EPR study of new azide and fluoride mononuclear Mn(III) complexes, J. Am. Chem. Soc. 125 (2003) 12337–12344, https://doi.org/10.1021/ja034652+.

[28] S. Romain, C. Duboc, F. Neese, E. Rivière, L. Hanton, A. Blackman, C. Philouze, J.-C. Leprêtre, A. Deronzier, M.-N. Collomb, An unusual stable mononuclear Mn(III) bis-terpyridine complex exhibiting Jahn-Teller compression: electrochemical synthesis, physical characterisation and theoretical study, Chem. Eur. J. 15 (4) (2009) 980–988, https://doi.org/10.1002/chem.200801442.

[29] S. Wang, W.-R. He, M. Ferbinteanu, Y.-H. Li, W. Huang, Tetragonally compressed high-spin Mn(III) Schiff base complex: Synthesis, crystal structure, magnetic properties and theoretical calculations, Polyhedron 52 (2013) 1199–1205, https://doi.org/10.1016/j.poly.2012.06.042.

[30] N. Berg, T.N. Hooper, J. Liu, C.C. Beedle, S.K. Singh, G. Rajaraman, S. Piligkos, S. Hill, E.K. Brechin, L.F. Jones, Synthetic, structural, spectroscopic and theoretical study of a Mn(III)–Cu(II) dimer containing a Jahn-Teller compressed Mn ion, Dalton Trans. 42 (2013) 207–216, https://doi.org/10.1039/C2DT31995K.

[31] S.J. Smith, M.J. Riley, C.J. Noble, G.R. Hanson, R. Stranger, V. Jayaratne, G. Cavigliasso, G. Schenk, L.R. Gahan, Structural and catalytic characterization of a heterovalent Mn(II)Mn(III) complex that mimics purple acid phosphatases, Inorg. Chem. 48 (21) (2009) 10036–10048, https://doi.org/10.1021/ic9005086.

[32] S. Shova, V. Tiron, A. Vlad, G. Novitchi, D.G. Dumitrescu, M. Damoc, M.-F. Zaltariov, M. Cazacu, Permethylated dinuclear Mn(III) coordination nanostructure with stripe-ordered magnetic domains, Appl. Organomet. Chem. 34 (12) (2020), https://doi.org/10.1002/aoc.v34.1210.1002/aoc.5957.

[33] A.K. Gregson, D.M. Doddrell, P.C. Healy, Low-temperature magnetic properties of three vanadium(III) and manganese(III) ß-diketonate complexes, Inorg. Chem. 17 (1978) 1216–1219, https://doi.org/10.1021/ic50183a025.

[34] C. Duboc, D. Ganyushin, K. Sivalingam, M.-N. Collomb, F. Neese, Systematic theoretical study of the zero-field splitting in coordination complexes of Mn(III). Density functional theory versus multireference wave function approaches, J. Phys. Chem. A. 114 (39) (2010) 10750–10758, https://doi.org/10.1021/jp107823s.

[35] M. Retegan, M.-N. Collomb, F. Neese, C. Duboc, A combined high-field EPR and quantum chemical study on a weakly ferromagnetically coupled dinuclear Mn(III) complex. A complete analysis of the EPR spectrum beyond the strong coupling limit, Phys. Chem. Chem. Phys. 15 (2013) 223–234, https://doi.org/10.1039/C2CP42955A.

[36] J. Krzystek, A. Schnegg, A. Aliabadi, K. Holldack, S.A. Stoian, A. Ozarowski, S. D. Hicks, M.M. Abu-Omar, K.E. Thomas, A. Ghosh, K.P. Caulfield, Z.J. Tonzetich, J. Telser, Advanced paramagnetic resonance studies on manganese and iron corroles with a formal d^4 electron count, Inorg. Chem. 59 (2) (2020) 1075–1090, https://doi.org/10.1021/acs.inorgchem.9b02635.

[37] S. Shova, A. Vlad, M. Cazacu, J. Krzystek, A. Ozarowski, M. Malček, L. Bucinsky, P. Rapta, J. Cano, J. Telser, V.B. Arion, Dinuclear manganese(III) complexes with bioinspired coordination and variable linkers showing weak exchange effects: a synthetic, structural, spectroscopic and computation study, Dalton Trans. 48 (2019) 5909–5922, https://doi.org/10.1039/C8DT04596H.

[38] J. Krzystek, J. Telser, J. Li, M.A. Subramanian, Magnetic properties and electronic structure of manganese-based blue pigments: a high-frequency and -field EPR study, Inorg. Chem. 54 (18) (2015) 9040–9045, https://doi.org/10.1021/acs.inorgchem.5b01306.

[39] J.P. Fackler, A. Avdeef, Crystal and molecular structure of tris(2,4-pentanedionato)manganese(III), $Mn(O_2C_5H_7)_3$, a distorted complex as predicted by Jahn-Teller arguments, Inorg. Chem. 13 (8) (1974) 1864–1875, https://doi.org/10.1021/ic50138a016.

[40] R.F. Ziolo, R.H. Stanford, G.R. Rossman, H.B. Gray, Synthesis and structural characterization of a new cyanomanganate(III) complex, heptapotassium.mu.-oxo-bis[pentacyanomanganate(III)]cyanide, J. Am. Chem. Soc. 96 (26) (1974) 7910–7915, https://doi.org/10.1021/ja00833a011.

[41] J.J. Alexander, H.B. Gray, Electronic structures of hexacyanometalate complexes, J. Am. Chem. Soc. 90 (16) (1968) 4260–4271, https://doi.org/10.1021/ja01018a013.

[42] I.D. Chawla, M.J. Frank, Electronic spectra of hexacyanomanganate(III) and hydroxopentacyanomanganate (III) ions in acidic media, J. Inorg. Nucl. Chem. 32 (2) (1970) 555–563, https://doi.org/10.1016/0022-1902(70)80265-2.

[43] W.P. Griffith, Cyanide complexes of the early transition metals (groups IVa-VIIa), Coord. Chem. Rev. 17 (2-3) (1975) 177–247, https://doi.org/10.1016/S0010-8545(00)80303-3.

[44] W.E. Buschmann, L. Liable-Sands, A.L. Rheingold, J.S. Miller, Structure and physical properties of hexacyanomanganate(III), [MnIII(CN)6]3, Inorg. Chim. Acta 284 (2) (1999) 175–179, https://doi.org/10.1016/S0020-1693(98)00284-9.

[45] L. Galich, H. Hückstädt, H. Homborg, Tetra(n -butyl)ammonium Dicyanotetraphenyl-porphyrinatomanganate(III); Crystal Structure and Electronic Resonance Raman and Absorption Spectra, J. Porphyr. Phthalocyanines. 02 (1998) 79–87. https://doi.org/10.1002/(SICI)1099-1409(199801/02)2:1<79::AID-JPP52>3.0.CO;2-7.

[46] J.T. Landrum, K. Hatano, W.R. Scheidt, C.A. Reed, Imidazolate complexes of iron and manganese tetraphenylporphyrins, J. Am. Chem. Soc. 102 (22) (1980) 6729–6735, https://doi.org/10.1021/ja00542a011.

[47] A.P. Hansen, H.M. Goff, Low-spin manganese(III) porphyrin imidazolate and cyanide complexes. Modulation of magnetic anisotropy by axial ligation, Inorg. Chem. 23 (26) (1984) 4519–4525, https://doi.org/10.1021/ic00194a023.

[48] M. Matsuda, J.-I. Yamaura, H. Tajima, T. Inabe, Structure and magnetic properties of a low-spin manganese(III) phthalocyanine dicyanide complex, Chem. Lett. 34 (11) (2005) 1524–1525, https://doi.org/10.1246/cl.2005.1524.

[49] S. Mossin, H.O. Sørensen, H. Weihe, trans -Bis(cyano-κ C)(1,4,8,11-tetraazacyclotetradecane-κ 4 N)manganese(III) perchlorate, a low-spin manganese(III) complex, Acta Crystallogr, Sect. C Cryst. Struct. Commun. 58 (4) (2002) m204–m206, https://doi.org/10.1107/S0108270102001713.

[50] H.E. Colmer, C.G. Margarit, J.M. Smith, T.A. Jackson, J. Telser, Spectroscopic and computational investigation of low-spin Mn(III) Bis(scorpionate) complexes, Eur. J. Inorg. Chem. 2016 (15–16) (2016) 2413–2423, https://doi.org/10.1002/ejic.v2016.15-1610.1002/ejic.201501250.

[51] A.P. Forshaw, J.M. Smith, A. Ozarowski, J. Krzystek, D. Smirnov, S.A. Zvyagin, T. D. Harris, H.I. Karunadasa, J.M. Zadrozny, A. Schnegg, K. Holldack, T.A. Jackson,

A. Alamiri, D.M. Barnes, J. Telser, Low-spin hexacoordinate Mn(III): synthesis and spectroscopic investigation of homoleptic tris(pyrazolyl)borate and tris (carbene)borate complexes, Inorg. Chem. 52 (1) (2013) 144–159, https://doi.org/10.1021/ic301630d.

[52] F. Hossain, M.A. Rigsby, C.T. Duncan, P.L. Milligan, R.L. Lord, M.-H. Baik, F. A. Schultz, Synthesis, structure, and properties of low-spin manganese(III)−poly (pyrazolyl)borate complexes, Inorg. Chem. 46 (2007) 2596–2603, https://doi.org/10.1021/ic062224+.

[53] D.C.L. De Alwis, F.A. Schultz, Metal−Bis[poly(pyrazolyl)borate] Complexes. Electrochemical, Magnetic, and Spectroscopic Properties and Coupled Electron-Transfer and Spin-Exchange Reactions, Inorg. Chem. 42 (2003) 3616–3622. https://doi.org/10.1021/ic034077a.

[54] P. Basu, A. Chakravorty, Low-spin tris(quinone oximates) of manganese(II, III). Synthesis, isomerism, and equilibria, Inorg. Chem. 31 (24) (1992) 4980–4986, https://doi.org/10.1021/ic00050a014.

[55] S. Ganguly, S. Karmakar, A. Chakravorty, First examples of carboxyl-bonded low-spin manganese(III) complexes, Inorg. Chem. 36 (1) (1997) 116–118, https://doi.org/10.1021/ic960485l.

[56] A. Barker, C.T. Kelly, I.A. Kühne, S. Hill, J. Krzystek, P. Wix, K. Esien, S. Felton, H. Müller-Bunz, G.G. Morgan, Spin state solvomorphism in a series of rare S = 1 manganese(iii) complexes, Dalton Trans. 48 (2019) 15560–15566, https://doi.org/10.1039/C9DT02476J.

[57] P. Greig Sim, E. Sinn, First manganese(III) spin crossover, first d^4 crossover. Comment on cytochrome oxidase, J. Am. Chem. Soc. 103 (1) (1981) 241–243, https://doi.org/10.1021/ja00391a067.

[58] I.A. Kühne, K. Esien, L.C. Gavin, H. Müller-Bunz, S. Felton, G.G. Morgan, Modulation of Mn^{3+} spin state by guest molecule inclusion, Molecules 25 (2020) 5603, https://doi.org/10.3390/molecules25235603.

[59] G.G. Morgan, K.D. Murnaghan, H. Müller-Bunz, V. McKee, C.J. Harding, A manganese(III) complex that exhibits spin crossover triggered by geometric tuning, Angew. Chem. Int. Ed. 45 (43) (2006) 7192–7195, https://doi.org/10.1002/anie.200601823.

[60] K. Pandurangan, B. Gildea, C. Murray, C.J. Harding, H. Müller-Bunz, G. G. Morgan, Lattice Effects on the spin-crossover profile of a mononuclear manganese(III) cation, Chem. Eur. J. 18 (7) (2012) 2021–2029, https://doi.org/10.1002/chem.201102820.

[61] B. Gildea, M.M. Harris, L.C. Gavin, C.A. Murray, Y. Ortin, H. Müller-Bunz, C. J. Harding, Y. Lan, A.K. Powell, G.G. Morgan, Substituent effects on spin state in a series of mononuclear manganese(III) complexes with hexadentate schiff-base ligands, Inorg. Chem. 53 (12) (2014) 6022–6033, https://doi.org/10.1021/ic5003012.

[62] B. Gildea, L.C. Gavin, C.A. Murray, H. Müller-Bunz, C.J. Harding, G.G. Morgan, Supramolecular modulation of spin crossover profile in manganese(III), Supramol. Chem. 24 (8) (2012) 641–653, https://doi.org/10.1080/10610278.2012.712120.

[63] I.A. Kühne, A. Barker, F. Zhang, P. Stamenov, O. O'Doherty, H. Müller-Bunz, M. Stein, B.J. Rodriguez, G.G. Morgan, Modulation of Jahn-Teller distortion and electromechanical response in a Mn^{3+} spin crossover complex, J. Phys. Condens. Matter. 32 (40) (2020) 404002, https://doi.org/10.1088/1361-648X/ab82d1.

[64] A.J. Fitzpatrick, E. Trzop, H. Müller-Bunz, M.M. Dîrtu, Y. Garcia, E. Collet, G. G. Morgan, Electronic vs. structural ordering in a manganese(III) spin crossover complex, Chem. Commun. 51 (2015) 17540–17543, https://doi.org/10.1039/C5CC05129K.

[65] P.N. Martinho, B. Gildea, M.M. Harris, T. Lemma, A.D. Naik, H. Müller-Bunz, T. E. Keyes, Y. Garcia, G.G. Morgan, Cooperative spin transition in a mononuclear manganese(III) complex, Angew. Chem. Int. Ed. 51 (50) (2012) 12597–12601, https://doi.org/10.1002/anie.201205573.

[66] V.B. Jakobsen, E. Trzop, L.C. Gavin, E. Dobbelaar, S. Chikara, X. Ding, K. Esien, H. Müller-Bunz, S. Felton, V.S. Zapf, E. Collet, M.A. Carpenter, G.G. Morgan, Stress-induced domain wall motion in a ferroelastic Mn^{3+} spin crossover complex, Angew. Chem. Int. Ed. 59 (32) (2020) 13305–13312, https://doi.org/10.1002/anie.202003041.

[67] V.B. Jakobsen, L. O'Brien, G. Novitchi, H. Müller-Bunz, A.-L. Barra, G.G. Morgan, Chiral resolution of a Mn^{3+} spin crossover complex, Eur. J. Inorg. Chem. 2019 (41) (2019) 4405–4411, https://doi.org/10.1002/ejic.201900765.

[68] C. Gandolfi, T. Cotting, P.N. Martinho, O. Sereda, A. Neels, G.G. Morgan, M. Albrecht, Synthesis and self-assembly of spin-labile and redox-active manganese(III) complexes, Dalton Trans. 40 (9) (2011) 1855, https://doi.org/10.1039/c0dt01222j.

[69] A.V. Kazakova, A.V. Tiunova, D.V. Korchagin, G.V. Shilov, E.B. Yagubskii, V. N. Zverev, S.C. Yang, J. Lin, J. Lee, O.V. Maximova, A.N. Vasiliev, The first conducting spin-crossover compound combining a Mn(III) cation complex with electroactive TCNQ demonstrating an abrupt spin transition with a hysteresis of 50 K, Chem. Eur. J. 25 (2019) 10204–10213, https://doi.org/10.1002/chem.201901792.

[70] S. Wang, M. Ferbinteanu, C. Marinescu, A. Dobrinescu, Q.-D. Ling, W. Huang, Case study on a rare effect: the experimental and theoretical analysis of a manganese(III) spin-crossover system, Inorg. Chem. 49 (21) (2010) 9839–9851, https://doi.org/10.1021/ic100364v.

[71] S. Wang, Y.-J. Li, F.-F. Ju, W.-T. Xu, K. Kagesawa, Y.-H. Li, M. Yamashita, W. Huang, The molecular and supramolecular aspects in mononuclear manganese (III) Schiff-base spin crossover complexes, Dalton Trans. 46 (2017) 11063–11077, https://doi.org/10.1039/C7DT01718A.

[72] J. Sirirak, D.J. Harding, P. Harding, K.S. Murray, B. Moubaraki, L. Liu, S.G. Telfer, Spin crossover in *cis* manganese(III) quinolylsalicylaldiminates, Eur. J. Inorg. Chem. 2015 (15) (2015) 2534–2542, https://doi.org/10.1002/ejic.201500196.

[73] M.S. Shongwe, K.S. Al-Barhi, M. Mikuriya, H. Adams, M.J. Morris, E. Bill, K. C. Molloy, Tuning a single ligand system to stabilize multiple spin states of manganese: a first example of a hydrazone-based manganese(III) spin-crossover complex, Chem. Eur. J. 20 (31) (2014) 9693–9701, https://doi.org/10.1002/chem.201402634.

[74] Z. Liu, S. Liang, X. Di, J. Zhang, A manganese(III) complex that exhibits spin crossover behavior, Inorg. Chem. Commun. 11 (7) (2008) 783–786, https://doi.org/10.1016/j.inoche.2008.03.030.

[75] C.-Y. Qin, S.-Z. Zhao, H.-Y. Wu, Y.-H. Li, Z.-K. Wang, Z. Wang, S. Wang, The dynamic interplay between intramolecular and intermolecular interactions in mononuclear manganese(III) SCO complexes, Dalton Trans. 50 (2021) 5899–5910, https://doi.org/10.1039/D0DT04109B.

[76] J. Olguín, Unusual metal centres/coordination spheres in spin crossover compounds, Coord. Chem. Rev. 407 (2020) 213148, https://doi.org/10.1016/j.ccr.2019.213148.

[77] A.L. Spek, PLATON SQUEEZE: a tool for the calculation of the disordered solvent contribution to the calculated structure factors, Acta Crystallogr. Sect. C Struct. Chem. 71 (2015) 9–18, https://doi.org/10.1107/S2053229614024929.

[78] S. Sundaresan, I. Kühne, C. Kelly, A. Barker, D. Salley, H. Müller-Bunz, A. Powell, G. Morgan, Anion influence on spin state in two novel Fe(III) compounds: [Fe(5F-Sal2-333)]X, Crystals 9 (2018) 19, https://doi.org/10.3390/cryst9010019.

[79] K.-ichiro. Motoda, H. Sakiyama, N. Matsumoto, H. Okawa, S. Kida, Template synthesis and structure of a dinuclear lead(II) complex of novel macrocycle derived from 2,6-diformyl-4-methylphenol and 1,9-diamino-3,7-diazanonane, Bull. Chem. Soc. Jpn. 65 (4) (1992) 1176–1178, https://doi.org/10.1246/bcsj.65.1176.

[80] M.G.B. Drew, C.J. Harding, V. McKee, G.G. Morgan, J. Nelson, Geometric control of manganese redox state, J. Chem. Soc. Chem. Commun. (10) (1995) 1035, https://doi.org/10.1039/c39950001035.

[81] R. Ketkaew, Y. Tantirungrotechai, P. Harding, G. Chastanet, P. Guionneau, M. Marchivie, D.J. Harding, OctaDist: a tool for calculating distortion parameters in spin crossover and coordination complexes, Dalton Trans. 50 (3) (2021) 1086–1096, https://doi.org/10.1039/D0DT03988H.

[82] I.A. Kühne, L.C. Gavin, M. Harris, B. Gildea, H. Müller-Bunz, M. Stein, G. G. Morgan, Mn(III) complexes with nitro-substituted ligands—Spin states with a twist, J. Appl. Phys. 129 (21) (2021) 213903, https://doi.org/10.1063/5.0050276.

[83] S. Tamburini, P.A. Vigato, D. Chiarello, P. Traldi, Mass spectrometric characterization of a barium thiocyanate complex with a new macrocycle, Inorg. Chim. Acta 156 (2) (1989) 271–275, https://doi.org/10.1016/S0020-1693(00)83511-2.

[84] M. Boča, P. Baran, R. Boča, G. Kickelbick, F. Renz, W. Linert, Imidazolidine ring-formation/cleavage due to intracomplex coordinative activation, Inorg. Chem. Commun. 2 (5) (1999) 188–190, https://doi.org/10.1016/S1387-7003(99)00044-1.

[85] M.G.B. Drew, J. Nelson, S. Martin Nelson, Metal-ion-controlled transamination in the synthesis of macrocyclic Schiff-base ligands. Part 2. Stepwise synthesis, ring expansion/contraction, and the crystal and molecular structure of a ten-co-ordinate barium(II) complex, J. Chem. Soc. Dalton Trans. (1981) 1678, https://doi.org/10.1039/dt9810001678.

[86] L.-W. Yang, S. Liu, E. Wong, S.J. Rettig, C. Orvig, Complexes of trivalent metal ions with potentially heptadentate N_4O_3 schiff base and amine phenol ligands of varying rigidity, Inorg. Chem. 34 (8) (1995) 2164–2178, https://doi.org/10.1021/ic00112a032.

[87] M.H. Habibi, E. Shojaee, G.S. Nichol, Synthesis, spectroscopic characterization and crystal structure of novel NNNN-donor μ-bis(bidentate) tetraaza acyclic Schiff base ligands, Spectrochim, Acta Part A Mol. Biomol. Spectrosc. 98 (2012) 396–404, https://doi.org/10.1016/j.saa.2012.08.064.

[88] C. Çelik, V. McKee, M. Köse, M. Aslantaş, M. Tümer, Crystal structure, spectroscopic and redox behaviour of novel imidazolidine ligand, J. Mol. Struct. 985 (2-3) (2011) 167–172, https://doi.org/10.1016/j.molstruc.2010.10.037.

[89] M. Fondo, A.M. García Deibe, N. Ocampo, M.R. Bermejo, J. Sanmartín, Dinuclear Cobalt(III) Complexes Showing a Co_2O_2 Metallacycle, Z. Anorg. Und Allg. Chem. 631 (11) (2005) 2041–2045, https://doi.org/10.1002/zaac.200570012.

[90] M.H. Habibi, N. Abarghooei-Shirazi, Y. Yamane, T. Suzuki, N , N ′-Bis(3-nitrobenzylidene)-2,2′-[2-(3-nitrophenyl)imidazolidine-1,3-diyl]diethanamine, Acta Crystallogr. Sect. E Struct. Reports Online. 66 (2010) o501–o501. https://doi.org/10.1107/S1600536810003168.

[91] F. Sancenón, A. Benito, J.M. Lloris, R. Martínez-Máñez, T. Pardo, J. Soto, ATP sensing with anthryl-functionalized open-chain polyaza-alkanes, Helv. Chim. Acta. 85 (2002) 1505, https://doi.org/10.1002/1522-2675(200205)85:5<1505::AID-HLCA1505>3.0.CO;2-K.

[92] Y. Feng, G. Liu, F. Yue, J.-D. Wang, N -[(2-Phenyl-2 H -1,2,3-triazol-4-yl) methylene]-2-(2-(2-phenyl-2 H-1,2,3-triazol-4-yl)-3-{2-[(2-phenyl-2 H-1,2,3-triazol-4-yl)methyleneamino]ethyl}imidazolidin-1-yl)ethanamine, Acta Crystallogr, Sect. C Cryst. Struct. Commun. 64 (8) (2008) o426–o427, https://doi.org/10.1107/S0108270108019033.

[93] R. Bikas, E. Shahmoradi, S. Reinoso, M. Emami, L. Lezama, J. Sanchiz, N. Noshiranzadeh, The effect of the orientation of the Jahn–Teller distortion on the magnetic interactions of trinuclear mixed-valence Mn(II)/Mn(III) complexes, Dalton Trans 48 (2019) 13799–13812, https://doi.org/10.1039/C9DT01652J.

[94] K. Pramanik, P. Malpaharia, E. Colacio, B. Das, S.K. Chandra, Octadentate flexible ligands as a platform for a variety of homo and heterometallic complexes containing diphenoxido and phenoxido/azido bridging groups: synthesis, structure and magnetic properties, New J. Chem. 42 (8) (2018) 6332–6342, https://doi.org/10.1039/C7NJ05112C.

[95] M. Fondo, N. Ocampo, A.M. García-Deibe, I. García-Santos, J. Sanmartín, A. J. Mota, J. Luis Pérez-Lustres, Ferromagnetic heterotrinuclear Cu–Ni complexes of a compartmental chiral Schiff base, Dalton Trans. 40 (44) (2011) 11770, https://doi.org/10.1039/c1dt10897b.

[96] M. Fondo, N. Ocampo, A.M. García-Deibe, J. Sanmartín, Zn_3, Ni_3, and Cu_3 Complexes of a Novel Tricompartmental Acyclic Ligand, Inorg. Chem. 48 (11) (2009) 4971–4979, https://doi.org/10.1021/ic900292h.

[97] N.A. Bailey, E.D. McKenzie, J.M. Worthington, M. McPartlin, P.A. Tasker, Molecular structure (X-ray analysis) of a dinuclear iron(III) compound formed with the $[N_4O_3]$ ligand 'Sal$_3$trien', Inorg. Chim. Acta 25 (1977) L137–L138, https://doi.org/10.1016/S0020-1693(00)95677-9.

[98] E.P. Copeland, I.A. Kahwa, J.T. Mague, G.L. McPherson, Novel mixed-valence vanadium(IV/V) molecule exhibiting unusual electron delocalization over the $[V_2O_3]^{3+}$ core, J. Chem. Soc. Dalton Trans. (1997) 2849–2852, https://doi.org/10.1039/a701356f.

[99] R. Bikas, E. Shahmoradi, N. Noshiranzadeh, M. Emami, S. Reinoso, The effects of halogen substituents on the catalytic oxidation of benzyl-alcohols in the presence of dinuclear oxidovanadium(IV) complex, Inorg. Chim. Acta 466 (2017) 100–109, https://doi.org/10.1016/j.ica.2017.05.049.

[100] N. Noshiranzadeh, M. Emami, R. Bikas, J. Sanchiz, M. Otręba, P. Aleshkevych, T. Lis, Synthesis, characterization and magnetic properties of a dinuclear oxidovanadium(IV) complex: magneto-structural DFT studies on the effects of out-of-plane –OCH_3 angle, Polyhedron. 122 (2017) 194–202, https://doi.org/10.1016/j.poly.2016.11.026.

[101] D.F. Back, G.M. de Oliveira, L.A. Fontana, A. Neves, B.A. Iglesias, T.P. Camargo, P.T. Campos, J.P. Vargas, New dioxidouranium (VI) and mixed-valence oxidovanadium (IV/V) coordination compounds with N, O-pentadentate ligands obtained from pyridoxal and triethylenetetramine, Inorg. Chim. Acta 428 (2015) 163–169, https://doi.org/10.1016/j.ica.2015.01.013.

[102] B. Chiari, O. Piovesana, T. Tarantelli, P.F. Zanazzi, Exchange interaction in multinuclear transition-metal complexes. 2. Synthesis and structural and magnetic studies of a dinuclear iron(III) derivative of the heptadentate Schiff base trisalicylidenetriethylenetetramine, Inorg. Chem. 21 (6) (1982) 2444–2448, https://doi.org/10.1021/ic00136a063.

[103] B. Chiari, O. Piovesana, T. Tarantelli, P.F. Zanazzi, Exchange interaction in multinuclear transition-metal complexes. 4. Relative magnetic coupling in hydroxo- and methoxo-bridged dinuclear complexes of iron(III) with the heptadentate Schiff base trisalicylidenetriethylenetetramine, Inorg. Chem. 22 (19) (1983) 2781–2784, https://doi.org/10.1021/ic00161a030.

[104] C.T. Zeyrek, A. Elmali, Y. Elerman, Synthesis, crystal structure, magnetic characterization and spectroscopic properties of a new dinuclear iron(III) complex asymmetrically bridged by a phenoxo and methoxo groups, Cryst. Res. Technol. 41 (5) (2006) 510–516, https://doi.org/10.1002/crat.200510614.

[105] M. Mikuriya, S. Ono, Y. Koyama, R. Mitsuhashi, M. Tsuboi, Crystal structure of μ-oxido-μ-phenolato-bridged dinuclear manganese(III) complex of Schiff-base ligand with bromido coordination, X-Ray Struct, Anal. Online. 37 (0) (2021) 9–11, https://doi.org/10.2116/xraystruct.37.9.

[106] M. Fondo, N. Ocampo, A.M. García-Deibe, M. Corbella, M.S. El Fallah, J. Cano, J. Sanmartín, M.R. Bermejo, Dinuclear Co(III)/Co(II) and Co(II)/Co(III) mixed-valent complexes: synthetic control of the cobalt oxidation level, Dalton Trans. (2006) 4905–4913, https://doi.org/10.1039/B609961K.

[107] A.M. García-Deibe, M. Fondo, J. Corredoira-Vázquez, M. Salah El Fallah, J. Sanmartín-Matalobos, Hierarchical assembly of antiparallel homochiral sheets formed by hydrogen-bonded helixes of a trapped-valence Co(II)/Co(III) Complex, Cryst. Growth Des. 17 (2) (2017) 467–473, https://doi.org/10.1021/acs.cgd.6b01269.s001.

[108] S. Paul, W.-T. Wong, D. Ray, Mono and bimetallic Co(III) Schiff base complexes: Coordination induced ligand imidazolidine ring cleavage and stabilization, Inorg. Chim. Acta. 372 (1) (2011) 160–167, https://doi.org/10.1016/j.ica.2011.03.058.

[109] A.R. Paital, M. Sarkar, M. Mikuriya, D. Ray, [(Tmp)Co_2L] complexes through preassembly on 2,6-diformyl- and 2,6-bis(benzylimino)-4-methylphenolate templates, Eur. J. Inorg. Chem. 2007 (30) (2007) 4762–4769, https://doi.org/10.1002/ejic.200700551.

[110] M.A. Kamyabi, F. Soleymani-Bonoti, F. Alirezaei, R. Bikas, N. Noshiranzadeh, M. Emami, M.S. Krawczyk, T. Lis, Electrocatalytic properties of a dinuclear cobalt (III) coordination compound in molecular oxygen reduction reaction, Appl. Organomet. Chem. 33 (12) (2019), https://doi.org/10.1002/aoc.v33.1210.1002/aoc.5214.

[111] M. Fondo, N. Ocampo, A.M. García-Deibe, R. Vicente, M. Corbella, M.R. Bermejo, J. Sanmartín, Self-assembly of a tetranuclear Ni 4 cluster with an S = 4 Ground State: the first 3d metal cluster bearing a μ 4 -η 2:η 2 -O, O Carbonate Ligand, Inorg. Chem. 45 (2006) 255–262, https://doi.org/10.1021/ic051194s.

[112] M. Fondo, A.M. García-Deibe, N. Ocampo, J. Sanmartín, M.R. Bermejo, A. L. Llamas-Saiz, Dinuclear nickel complexes with a Ni_2O_2 core: a structural and magnetic study, Dalton Trans. (35) (2006) 4260–4270, https://doi.org/10.1039/B606414K.

[113] M. Fondo, A.M. García-Deibe, N. Ocampo, J. Sanmartín, M.R. Bermejo, Asymmetric self-assembly with atmospheric CO_2 fixation of a pentanuclear carbonate Ni(II) complex based on dissimilar building blocks, Dalton Trans. (4) (2007) 414–416, https://doi.org/10.1039/B617374H.

[114] L.-P. Lu, X.-P. Lu, M.-L. Zhu, Aqua-1κ O -{μ-1,3-bis[2-(2-oxidobenzylideneamino) ethyl]-2-(2-oxidophenyl)imidazolidine-1κ 4 O, N, N ′, O ′;2κ 4 O ′, N ′′, N ′′′, O ′′} (μ-2-formylphenolato-1:2κ 3 O 1: O 1, O 2)dinickel(II) trihydrate: a one-dimensional chain linked by O—H...O hydrog, Acta Crystallogr. Sect. C Cryst. Struct. Commun. 63 (2007) m374–m376, https://doi.org/10.1107/S0108270107023256.

[115] A.R. Paital, W.T. Wong, G. Aromí, D. Ray, New $[LNi(II)_2]^+$ complexes incorporating 2-formyl or 2,6-diformyl-4-methyl phenol as Inhibitors of the Hydrolysis of the Ligand L3-: Ni···Ni Ferromagnetic Coupling and S = 2 Ground States, Inorg. Chem. 46 (2007) 5727–5733, https://doi.org/10.1021/ic700496c.

[116] M. Fondo, N. Ocampo, A.M. García-Deibe, E. Ruíz, J. Tercero, J. Sanmartín, Discovering the complex chemistry of a simple Ni(II)/H_3L system: magnetostructural characterization and DFT calculations of di- and polynuclear nickel(II) compounds, Inorg. Chem. 48 (20) (2009) 9861–9873, https://doi.org/10.1021/ic9014916.

[117] A.R. Khan, Y. Tesema, R.J. Butcher, Y. Gultneh, μ-Acetato-μ-(5-chloro-2-{1,3-bis [2-(5-chloro-2-oxidobenzylideneamino)ethyl]imidazolidin-2-yl}phenolato)-bis [methanolnickel(II)] methanol monosolvate monohydrate, Acta Crystallogr, Sect. E Struct. Reports Online. 67 (9) (2011) m1264–m1265, https://doi.org/10.1107/S1600536811032727.

[118] K. Kumar, A. Kumar Dhara, V. Kumar Chaudhary, N. Sandip, P. Roy, P. Verma, K. Ghosh, The influence of the tertiary butyl group in the ligand frame on the catalytic activities, DNA cleavage ability and cytotoxicity of dinuclear nickel(II) complexes, Inorg. Chim. Acta 495 (2019) 118993, https://doi.org/10.1016/j.ica.2019.118993.

[119] M. Fondo, A.M. García-Deibe, M. Corbella, J. Ribas, A. Llamas-Saiz, M. R. Bermejo, J. Sanmartín, Ferromagnetic exchange in a dinuclear copper(II) complex mediated by a methanolate bridging ligand, Dalton Trans. (2004) 3503–3507, https://doi.org/10.1039/B410522B.

[120] M. Bera, W.T. Wong, G. Aromí, D. Ray, μ-η1:η1-N, N'-imidazolidine-bridged dicopper(II/III) complexes of a new dinucleating μ-bis(tetradentate) Schiff base ligand: synthesis, structural characterization, ^{1}H NMR spectroscopy, and magnetic coupling, Eur. J. Inorg. Chem. 2005 (12) (2005) 2526–2535, https://doi.org/10.1002/ejic.200500084.

[121] M. Fondo, N. Ocampo, A.M. García-Deibe, M. Corbella, M.R. Bermejo, J. Sanmartín, Ferromagnetism in dinuclear copper(II)-phenolate complexes with exogenous O-donor bridges: a comparative study, Dalton Trans. (23) (2005) 3785, https://doi.org/10.1039/b507068f.

[122] P.K. Nanda, M. Bera, G. Aromí, D. Ray, Atmospheric CO_2 fixation leads to a unique bridged complex and coordination induced ligand hydrolysis to a [Cu(II)] complex, Polyhedron 25 (14) (2006) 2791–2799, https://doi.org/10.1016/j.poly.2006.04.005.

[123] M. Fondo, N. Ocampo, A.M. García-Deibe, J. Sanmartín, Ferromagnetic tetranuclear and pentanuclear copper(II) complexes constructed from Cu_2 blocks, Eur. J. Inorg. Chem. 2010 (16) (2010) 2376–2384, https://doi.org/10.1002/ejic.201000057.

[124] A.A. Leitch, K. Lekin, S.M. Winter, L.E. Downie, H. Tsuruda, J.S. Tse, M. Mito, S. Desgreniers, P.A. Dube, S. Zhang, Q. Liu, C. Jin, Y. Ohishi, R.T. Oakley, From magnets to metals: the response of tetragonal bisdiselenazolyl radicals to pressure, J. Am. Chem. Soc. 133 (15) (2011) 6051–6060, https://doi.org/10.1021/ja200391j.

[125] A.R. Paital, J. Ribas, Leoní.A. Barrios, G. Aromí, D. Ray, Dissymmetry of an exogenous bridging ligand facilitates the assembly of a ferromagnetic and chiral [Cu(II)Ni(II)] complex, Dalton Trans. (2) (2009) 256–258, https://doi.org/10.1039/B811788H.

[126] B. Djukic, P.K. Poddutoori, P.A. Dube, T. Seda, H.A. Jenkins, M.T. Lemaire, Bimetallic Iron(III) spin-crossover complexes containing a 2,2′-bithienyl bridging bis-QsalH ligand, Inorg. Chem. 48 (13) (2009) 6109–6116, https://doi.org/10.1021/ic9004938.

[127] P.K. Nanda, V. Bertolasi, G. Aromí, D. Ray, Aqua bridged Cu_2 dimer of a heptadentate N_4O_3 coordinating ligand: synthesis, structure and magnetic properties, Polyhedron 28 (5) (2009) 987–993, https://doi.org/10.1016/j.poly.2008.12.063.

[128] M. Mikuriya, Y. Sato, D. Yoshioka, μ-phenolato-μ-acetato-bridged dinuclear copper(II) complex with dinucleating Schiff-base ligand having three phenolate groups, X-Ray Struct. Anal. Online 34 (0) (2018) 45–47, https://doi.org/10.2116/xraystruct.34.45.

[129] C. Liu, M.-X. Chen, M. Li, Synthesis, crystal structures, catalytic application and antibacterial activities of Cu(II) and Zn(II) complexes bearing salicylaldehyde-imine ligands, Inorg. Chim. Acta 508 (2020) 119639, https://doi.org/10.1016/j.ica.2020.119639.

[130] U. Mukhopadhyay, L. Govindasamy, K. Ravikumar, D. Velmurugan, D. Ray, Synthesis and structural characterization of a triply bridged copper(II)–zinc(II) Schiff base complex with N, O coordination, Inorg. Chem. Commun. 1 (4) (1998) 152–154, https://doi.org/10.1016/S1387-7003(98)00040-9.

[131] X.-P. Lu, M.-L. Zhu, L.-P. Lu, (μ-Acetato){μ-1,3-bis[2-(2-oxidobenzylideneamino) ethyl]-2-(2-oxidophenyl)-1,3-imidazolidine}dizinc(II) ethanol disolvate dihydrate, Acta Crystallogr, Sect. E Struct. Reports Online 65 (7) (2009) m729–m730, https://doi.org/10.1107/S1600536809020716.

[132] M. Fondo, A.M. García-Deibe, N. Ocampo, J. Sanmartín, M.R. Bermejo, Insights into the absorption of carbon dioxide by zinc substrates: isolation and reactivity of di- and tetranuclear zinc complexes, Dalton Trans. (14) (2004) 2135–2141, https://doi.org/10.1039/B405744A.

[133] M. Fondo, A.M. García-Deibe, N. Ocampo, J. Sanmartín, M.R. Bermejo, Influence of some reaction conditions on the obtaining of tetra- and dinuclear zinc complexes of some Schiff bases derived from 2,6-diformyl-4-alkyl-phenols, Polyhedron. 27 (12) (2008) 2585–2594, https://doi.org/10.1016/j.poly.2008.05.016.

[134] A.M. García-Deibe, M. Fondo, N. Ocampo, J. Sanmartín, E. Gómez-Fórneas, Design of chiral homodinuclear complexes based on the coordinating behaviour of some symmetric ligands, New J. Chem. 34 (6) (2010) 1073, https://doi.org/10.1039/c0nj00071j.

[135] J. He, Y.-G. Yin, X.-C. Huang, D. Li, Solid structure and photoluminescence of zinc (II) multiplex with heptadentate salicylideneamine as primary ligand, Inorg. Chem. Commun. 9 (2) (2006) 205–207, https://doi.org/10.1016/j.inoche.2005.11.003.
[136] M. Fondo, A.M. García-Deibe, N. Ocampo, J. Sanmartín, M.R. Bermejo, E. Oliveira, C. Lodeiro, From dinuclear to tetranuclear zinc complexes through carboxylate donors: structural and luminescence studies, New J. Chem. 32 (2) (2008) 247–257, https://doi.org/10.1039/B710660B.
[137] T. Singha Mahapatra, A. Roy, S. Chaudhury, S. Dasgupta, S. Lal Shrivastava, V. Bertolasi, D. Ray, Trapping of a methanoato bridge in μ-1,1,3,3 Mode for [Cu_4] aggregate formation: synthesis, steric control on nuclearity, antimicrobial activity, and DNA-interaction properties, Eur. J. Inorg. Chem. 2017 (4) (2017) 769–779, https://doi.org/10.1002/ejic.201601092.
[138] A.R. Paital, C.S. Hong, H.C. Kim, D. Ray, [Cu(II)$_4$] clusters from the self-assembly of two imidazolidinyl 2-phenolate-bridged [$Cu(II)_2$] units: the role of the chloride bridge, Eur. J. Inorg. Chem. 2007 (12) (2007) 1644–1653, https://doi.org/10.1002/ejic.200600917.
[139] A.R. Paital, V. Bertolasi, G. Aromí, J. Ribas-Ariño, D. Ray, A novel [Cu(II)$_4$] cluster from the assembly of two [$Cu(II)_2$L]+ units by a central μ 4–1,1,2,2 perchlorate ligand, Dalton Trans. (7) (2008) 861–864, https://doi.org/10.1039/B715768A.
[140] M. Fondo, A.M. García-Deibe, M. Corbella, E. Ruiz, J. Tercero, J. Sanmartín, M. R. Bermejo, Unexpected Ferromagnetic interaction in a new tetranuclear copper (II) complex: synthesis, crystal structure, magnetic properties, and theoretical studies, Inorg. Chem. 44 (2005) 5011–5020, https://doi.org/10.1021/ic0482741.
[141] P.K. Nanda, G. Aromí, D. Ray, Tetranuclear Cu(II) complex supported by a central μ4 -1,1,3,3 azide bridge, Chem. Commun. (2006) 3181–3183, https://doi.org/10.1039/B604502B.
[142] M. Fondo, A.M. García-Deibe, M.R. Bermejo, J. Sanmartín, A.L. Llamas-Saiz, Spontaneous carbon dioxide fixation: a μ4-carbonate bridged tetranuclear zinc(II) complex of a heptadentate Schiff base, J. Chem. Soc. Dalton Trans. (24) (2002) 4746, https://doi.org/10.1039/b209328f.
[143] A. Sarkar, A.R. Paital, R.A. Khan, F. Arjmand, V. Bertolasi, C. Mathonière, R. Clérac, D. Ray, Ligand dependent self-assembly of hydroxido-bridged dicopper units templated by sodium ion, Dalton Trans. 42 (34) (2013) 12495, https://doi.org/10.1039/c3dt51095f.
[144] K. Pramanik, P. Malpaharia, A.J. Mota, E. Colacio, B. Das, F. Lloret, S.K. Chandra, Stepwise formation of a pentanuclear Ni_4Cu Heterometallic complex exhibiting a vertex-sharing defective double-cubane core and diphenoxo- and phenoxo/azide bridging groups: a magnetostructural and DFT theoretical study, Inorg. Chem. 52 (7) (2013) 3995–4001, https://doi.org/10.1021/ic302784q.
[145] M. Fondo, N. Ocampo, A.M. García-Deibe, J. Cano, J. Sanmartín, One pot-synthesis of chiral Ni_6 clusters involving Ni_3 subunits: a combined structural, magnetic and DFT study, Dalton Trans. 39 (45) (2010) 10888, https://doi.org/10.1039/c0dt00659a.
[146] M. Fondo, J. Corredoira-Vázquez, A. Herrera-Lanzós, A.M. García-Deibe, J. Sanmartín-Matalobos, J.M. Herrera, E. Colacio, C. Nuñez, Improving the SMM and luminescence properties of lanthanide complexes with LnO_9 cores in the presence of Zn(II) : an emissive Zn_2Dy single ion magnet, Dalton Trans 46 (2017) 17000–17009, https://doi.org/10.1039/C7DT03438E.
[147] J. Corredoira-Vázquez, M. Fondo, J. Sanmartín-Matalobos, A.M. García-Deibe, 2D supramolecular structure for a chiral heterotrinuclear $Zn(II)_2Ho(III)$ complex through varied HBonds connecting solvates and counterions, IECC Proceedings. 2 (2018) 1114, https://doi.org/10.3390/IECC_2018-05247.
[148] M. Fondo, A.M. García-Deibe, J. Sanmartín, M.R. Bermejo, L. Lezama, T. Rojo, A Binuclear Copper(II) Acetate Complex Showing a 3D Supramolecular Network with Hydrophilic Pockets: Its Unusual Magnetic Behaviour, Eur. J. Inorg. Chem. 2003 (2003) 3703–3706. https://doi.org/10.1002/ejic.200300478.
[149] K. Sakata, T. Yamamoto, M. Hashimoto, X. Shen, A. Tsuge, H. Kuma, Synthesis and characterization of yttrium(III), lanthanum(III), and holmium(III) complexes with a heptadentate Schiff base ligand, Synth. React. Inorg. Met. Chem. 34 (4) (2004) 641–651, https://doi.org/10.1081/SIM-120035947.
[150] L. Zhang, F. Jiang, Y. Zhou, Structures and fluorescence of two new hetero-dinuclear lanthanide(III) complexes derived from a Schiff-base ligand, J. Coord. Chem. 62 (9) (2009) 1476–1483, https://doi.org/10.1080/00958970802596383.
[151] Z. Lijuan, Z. Yunshan, J. Fei, Structure and fluorescence of three new homodinuclear lanthanide (III)/Schiff-base compounds [{Ln(clapi)}$_2$]·2CH_3CN {Ln=La, Ce, Eu; H3clapi = 2-(5-Cchloride-2-hydroxyphenyl)-1,3-bis [4-(5-chloride-2-hydroxyphenyl)-3-azabut-3-enyl]-1,3-imidazolidine}, J. Chem. Crystallogr. 38 (2008) 595–599, https://doi.org/10.1007/s10870-008-9351-9.
[152] J. Chakraborty, S. Thakurta, G. Pilet, R.F. Ziessel, Loïc.J. Charbonnière, S. Mitra, Syntheses, crystal structures and photophysical properties of two doubly μ-phenoxo-bridged Ln(III) (Ln = Pr, Nd) homodinuclear Schiff base complexes, Eur. J. Inorg. Chem. 2009 (26) (2009) 3993–4000, https://doi.org/10.1002/ejic.200900251.
[153] Q.-F. Xie, M.-L. Huang, Y.-M. Chen, bis{μ-1 3-bis[2-(5-bromo-2-oxidobenzylideneamino)ethyl]-2-(5-bromo-2-oxidophenyl)-1, 3-imidazolidine}dineodymium (III) N, N -dimethylformamide hexasolvate, Acta Crystallogr. Sect. E Struct. Reports Online. 65 (2009), https://doi.org/10.1107/S1600536809047564 m1660–m1660.
[154] R.C. Howell, K.V.N. Spence, I.A. Kahwa, D.J. Williams, Structure and luminescence of the neutral dinuclear lanthanide(III) complexes [{Ln(api)}$_2$] {H_3api = 2-(2-hydroxyphenyl)-1,3-bis[4-(2-hydroxyphenyl)-3-azabut-3-enyl]-1,3-imidazolidine}, J. Chem. Soc. Dalton Trans. (1998) 2727–2734, https://doi.org/10.1039/a804056g.
[155] Z. Jiang, L. Sun, M. Li, H. Wu, Z. Xia, H. Ke, Y. Zhang, G. Xie, S. Chen, Solvent-tuned magnetic exchange interactions in Dy_2 systems ligated by a μ-phenolato heptadentate Schiff base, RSC Adv. 9 (68) (2019) 39640–39648, https://doi.org/10.1039/C9RA08754K.
[156] Z. Jiang, L. Sun, Q. Yang, S. Wei, H. Ke, S. Chen, Y. Zhang, Q. Wei, G. Xie, Solvent orientation in the crystal lattice producing distinct magnetic dynamics in two binuclear Dy(III) polymorphs with a polydentate Schiff base ligand, CrystEngComm. 19 (2017) 5735–5741, https://doi.org/10.1039/C7CE01269A.
[157] L. Zhao, J. Wu, H. Ke, J. Tang, Three dinuclear lanthanide(III) compounds of a polydentate Schiff base ligand: Slow magnetic relaxation behaviour of the Dy(III) derivative, CrystEngComm 15 (26) (2013) 5301, https://doi.org/10.1039/c3ce40153g.
[158] R.C. Clark, J.S. Reid, The analytical calculation of absorption in multifaceted crystals, Acta Crystallogr. Sect. A 51 (6) (1995) 887–897, https://doi.org/10.1107/S0108767395007367.
[159] G.M. Sheldrick, Crystal structure refinement with SHELXL, Acta Crystallogr. Sect. C Struct. Chem. 71 (2015) 3–8, https://doi.org/10.1107/S2053229614024218.